Paleomagnetic constraints on the timing and distribution of Cenozoic rotations in Central and Eastern Anatolia

Derya Gürer[1], Douwe J.J. van Hinsbergen[1], Murat Özkaptan[2], Iverna Creton[1], Mathijs R. Koymans[1], Antonio Cascella[3], Cornelis G. Langereis[1]

[1]Department of Earth Sciences, University of Utrecht, Utrecht 3584 CD, The Netherlands
[2]Department of Geophysical Engineering, Karadeniz Technical University, Trabzon 61080, Turkey
[3]Istituto Nazionale di Geofisica e Vulcanologia (INGV), Pisa 56126, Italy

Correspondence to: D. Gürer (derya.guerer@gmail.com)

Abstract. To quantitatively reconstruct the kinematic evolution of Central and Eastern Anatolia within the framework of Neotethyan subduction accommodating Africa-Eurasia convergence, we paleomagnetically assess timing and amount of vertical axis rotations across the Ulukışla and Sivas regions. We show paleomagnetic results from ~30 localities identifying a coherent rotation of a SE Anatolian rotating block - comprising the southern Kırşehir Block, the Ulukışla Basin, the Central and Eastern Taurides, and the southern part of the Sivas Basin. Using our new and published results, we compute an apparent polar wander path (APWP) for this block since the Late Cretaceous, showing that it experienced a ~30-35° counter-clockwise vertical axis rotation since Oligocene time relative to Eurasia. Sediments in the northern Sivas region show clockwise rotations. We use the rotation patterns together with known fault zones to argue that the counter-clockwise rotating domain of south-central Anatolia was bounded by the Savcılı Thrust Zone and Deliler-Tecer Fault Zone in the north and by the African-Arabian trench in the south, the western boundary of which is poorly constrained and requires future study. Our new paleomagnetic constraints provide a key ingredient for future kinematic restorations of the Anatolian tectonic collage.

1 Introduction

The Anatolian orogen in the eastern Mediterranean region comprises a complex collage of ocean- and continent-derived crustal units that amalgamated during Africa-Eurasia convergence and associated subduction since the Mesozoic, and that today forms a nascent orogenic plateau (e.g. Schildgen et al., 2012). One of the most striking features in Anatolian geology are two major strike-slip faults along which Anatolia is moving westwards relative to Eurasia, associated with major seismicity. This complex orogen with its major seismic hazards has been extensively studied to develop dynamic concepts to explain late Neogene escape tectonics (e.g. Gürsoy et al., 2011) and plateau rise, and in deeper geological time, for e.g. subduction initiation and evolution (e.g. Gürer et al., 2016).

An essential ingredient for analysis of the geodynamic underpinnings of orogenic evolution is a detailed kinematic restoration of deformation that culminated in today's orogen. Quantitative kinematic data for such reconstructions come from global plate reconstructions to constrain convergence through time, structural geology to estimate timing, style, and amount of fault displacements in the orogen, and paleomagnetic constraints on amount, distribution, and timing of vertical axis block rotations. Together, such constraints allow estimating how convergence was partitioned over the orogen, and help to identify the location, timing, and amount of e.g. subduction during orogenesis.

The Anatolian collage may in its simplest form be subdivided in two major belts (**Fig. 1**): the Pontide fold-and-thrust belt in the north, which has formed the southern Eurasian margin since at least the mid Mesozoic (Dokuz et al., 2017; Nikishin et al., 2015; Şengör and Yılmaz, 1981; Ustaömer and Robertson, 2010, 1997), and the Anatolide-Tauride belt in the south. This latter belt is thought to have derived from a microcontinental realm that was separated from Eurasia and Africa by ocean

basins, and consists of metamorphosed and non-metamorphosed tectonic units overlain by Cretaceous ophiolites. In Central Anatolia, the wider Anatolide-Tauride belt consists of (from north to south) the Kırşehir Block, the Afyon Zone, and the Tauride fold-and-thrust belt (**Fig. 1,** Barrier and Vrielynck, 2008; Boztuğ et al., 2009; Menant et al., 2016; Moix et al., 2008; Parlak et al., 2012; Robertson, 2002; Robertson et al., 2009; van Hinsbergen et al., 2016). Ages of accretion,

5   metamorphism and exhumation are younging from north to south, and range from Late Cretaceous to Eocene (Göncüoglu, 1997; Gürer et al., 2016; Okay and Tüysüz, 1999; van Hinsbergen et al., 2016). The Pontide and Anatolide-Tauride belts are separated by the Izmir-Ankara-Erzincan suture zone (IAESZ) that demarcates the former location of the now subducted Neotethys Ocean and that is thought to result from latest Cretaceous to Paleogene collision of the Anatolide-Tauride and Pontide belts (**Fig. 1**; Şengör and Yılmaz, 1981).

10 Previous paleomagnetic research has revealed that these major continent-derived units were in Cenozoic time broken up into large structural blocks that underwent significant vertical axis rotations relative to one another, bounded by fault zones. The Pontides of Central Anatolia were deformed in Paleogene time into a northward convex orocline (Meijers et al., 2010; Kaymakci et al., 2003; Cinku et al., 2011; Lucifora et al., 2016). Deformation was accommodated along thrusts associated with the IAESZ in the south, and thrusts inverting the southern Black Sea margin in the north (Kaymakci et al.,

15 2009; Espurt et al., 2014) (**Fig. 1**). To the south, the Kırşehir Block broke into three rotating blocks: the northeastern Akdağ-Yozgat Block (AYB), the central Kırşehir-Kırıkkale Block (KKB), and the southern Avanos-Ağacören Block (AAB) as shown by paleomagnetic data from Upper Cretaceous granitoids (Lefebvre et al., 2013). These rotating blocks were bordered by transpressional fault zones active between the Late Eocene and Early Miocene (e.g. Gülyüz et al., 2013; Advokaat et al., 2014; Isik et al., 2014). In southern and eastern Anatolia, large rotations have been identified in the Taurides and overlying

20 sedimentary basins (Çinku et al., 2016; Kissel et al., 2003, 1993, Meijers et al., 2016, 2011; Piper et al., 2002a, **Fig. 1**), but the regional coherence, block size, and bounding structures that accommodated these rotations are poorly defined.

In this paper, we aim to constrain the dimension of the Cenozoic rotating domain(s) in central and eastern Anatolia, the timing of their rotation, and the structures that may have accommodated these rotations relative to surrounding blocks. To this end, we collected new paleomagnetic data from two major, uppermost Cretaceous to Miocene sedimentary basins

25 that overlie the Taurides and Kırşehir blocks: the Ulukışla and Sivas basins (**Fig. 1**). We combine our extensive new dataset with existing data to identify the dimension of rotating domains in Central and Eastern Anatolia, and identify structures that may have accommodated these rotations.

2 Geological setting

2.1 Basement units

30 The Pontides mountain belt in northern Turkey contains Gondwana-derived fragments which had collided with Eurasia by mid-Mesozoic time (e.g. Okay and Nikishin, 2015; e.g., Şengör and Yılmaz, 1981; Ustaömer and Robertson, 1997; Ustaömer and Robertson, 2010; Dokuz et al., 2017). Since at least Early Jurassic time, the Pontides became bounded to the south by a northward dipping subduction zone (Okay et al., 2014; Topuz et al., 2014) that consumed Mesozoic Neotethyan oceanic crust.

35 The Kırşehir Block became underthrusted and metamorphosed in Late Cretaceous time, around 85-90 Ma due to ophiolite emplacement (Boztuğ et al., 2009; Whitney and Hamilton, 2004). Subsequently, around 70-65 Ma the Afyon Zone was accreted and metamorphosed (Özdamar et al., 2013; Pourteau et al., 2013). This was followed by the latest Cretaceous to Eocene accretion of the Tauride fold-and-thrust belt that largely consists of carbonate nappes (Demirtasli et al., 1984; Gutnic et al., 1979; Monod, 1977; Özgül, 1984). The Taurides mostly escaped metamorphism and accreted while the

Kırşehir Block and Afyon Zone were exhumed by extension in Late Cretaceous to Early Eocene time (Gautier et al., 2008, 2002; Gürer et al., 2018; Isik, 2009; Isik et al., 2008; Lefebvre et al., 2015, 2011).

After the latest Cretaceous to Paleocene onset of collision of the Kırşehir Block with the Pontides, and the closure of the IAESZ (Kaymakci et al., 2009), the Pontides as well as the Kırşehir Block broke into large blocks that rotated relative to each other. This started with formation of the Pontides orocline in the Paleogene (Meijers et al., 2010). Further shortening and vertical axis rotations moved to the south (Çankırı Basin, **Fig. 1**) and continued until the Early Miocene (Kaymakci et al., 2003; 2009; Lucifora et al., 2013; Espurt et al., 2014). East of the orocline and north of the Sivas Basin, the Pontides did not experience significant rotation since the Eocene (Meijers et al., 2010a and references therein).

The Kırşehir Block broke into three sub-blocks separated by fault zones (Lefebvre et al., 2013, **Fig. 1**). The AAB in the south and KKB in the northwest were separated by the Savcılı Thrust Zone (STZ) - a sinistral structure that underwent contraction between ~40 Ma and at least ~23 Ma (Isik et al., 2014; Advokaat et al., 2014), and the KKB and the AYB in the northeast were separated by the Delice-Kozakli Fault Zone (DKFZ) that was postulated to be a dextral, transpressional structure with an estimated offset of up to 90 km (Lefebvre et al., 2013, **Fig. 1**). To the west, the Kırşehir Block is bordered by the Tuzgölü Fault Zone (TFZ, **Fig. 1**), which contains a large normal fault displacement of at least Eocene and younger age (Çemen et al., 1999).

The Taurides to the south are bent into an orocline, with clockwise rotations in the western Central Taurides (Kissel et al., 1993; Meijers et al., 2011; Çinku et al., 2016; Piper et al., 2002) and counter-clockwise rotations reported from the Eastern Taurides (Çinku et al., 2016; Kissel et al., 2003). The Eastern Taurides are cut by NNE-SSW trending strike slip faults. The most western of these is the Ecemiş Fault Zone (EFZ; **Figs 1, 2)** that separates the Kırşehir Block and Central Taurides to the west, and the Eastern Taurides to the east (e.g. Jaffey and Robertson, 2001). It also left-laterally disrupts the connection between the Ulukışla and Sivas basins from Eocene-Oligocene time onward (Gürer et al., 2016). To the south, Lower Miocene sediments in the Adana Basin (A in **Fig. 1**) seal the strike-slip component of the Ecemiş Fault Zone, which after Early Miocene time only experienced E-W directed normal faulting with only a minor strike-slip component (Alan et al., 2011; Higgins et al., 2015; Jaffey and Robertson, 2001; Sarıkaya et al., 2015).

2.2 Sedimentary basins flanking the northern Taurides

Several sedimentary basins developed on top of the sutures and recorded the geological evolution of the Anatolian orogen from the Late Cretaceous to present. Broad similarities in their stratigraphy suggest that the Upper Cretaceous-Paleogene stratigraphic record of the Ulukışla and Sivas basins once formed a contiguous basin. Both overlie the Cretaceous ophiolites and contain stratigraphies that overlap in time with thrusting, metamorphism, exhumation, and accretion of the underlying Tauride units (Akyuz et al., 2013; Clark and Robertson, 2005, 2002; Gürer et al., 2016; Poisson et al., 1996).The Ulukışla and Sivas basins became separated due to displacement along the Ecemis Fault Zone in the Late Eocene-Oligocene (**Figs. 1-3**).

The Ulukışla Basin (**Fig. 2**) contains a discontinuous stratigraphic record of laterally variable series of shallow and deeper marine clastic and carbonate sediments interlayered with volcanic rocks, overlain by continental coarse clastic rocks. The deposits range from latest Cretaceous to Miocene in age and unconformably overlie ophiolitic basement. Eocene and younger rocks of the basin also unconformably overlie metamorphic rocks of the Kırşehir Block and the Afyon Zone. In Late Cretaceous time, the basin developed above the Alihoca ophiolites, during the burial of the Afyon Zone below these

ophiolites. From this context, the basin is interpreted as a forearc basin. During extensional exhumation of the Afyon Zone along the top-to-the-north Ivriz Detachment (**Fig. 1**) , the basin underwent N-S extension in the detachment's hanging wall and underwent widespread marine clastic deposition (Gürer et al., 2018, 2016). At the northern basin margin and close to the contact with the Kırşehir Block, a series of large-offset listric normal faults are compatible with E-W extension (in present-day coordinates). These offset sediments and the base of Paleocene volcanics indicate that E-W extension occurred simultaneously with N-S extension in the south, which prevailed until at least 56 Ma (Gürer et al., 2016). Following extension and exhumation, the Late Eocene-Oligocene history of the basin involved N-S shortening in especially the southern part of the basin, resulting in the formation of a north-verging fold with a widely exposed subvertical to overturned northern limb that marks the southern exposures of the Ulukışla Basin, and subordinate top-to-the-south thrusting in the synclinal hinge zone. Westward, these folds become more open and structures become gradually NE-SW oriented, while several anticlines and synclines deform the basal stratigraphy of the basin. The Oligocene redbeds in the Aktoprak syncline (Meijers et al., 2016) in the southwestern part of the Ulukışla Basin are interpreted as having been deposited during folding (Gürer et al., 2016). To the east, the folded Ulukışla Basin sediments curve towards NE-SW strikes interpreted to reflect drag folding against the major left-lateral EFZ (Gürer et al., 2016).

The Sivas region (**Figs 1, 3**) hosts a depocenter which is bound by the Pontides to the north, the Kırşehir Block/EFZ in the west, and the Taurides in the south. Its eastern boundary is diffuse. To the south, on the northern flanks of the Tauride fold-and-thrust belt, ophiolites are unconformably overlain by uppermost Cretaceous to Eocene, dominantly marine carbonate and clastic sediments and Paleocene volcanic and volcaniclastic rocks. These sediments were affected by north-verging Paleocene-Eocene thrusting (Cater et al., 1991; Poisson et al., 1996; Yilmaz and Yilmaz, 2006), possibly related to so far structurally poorly reconstructed thrusting in the Tauride fold-and-thrust belt underneath. In the Late Eocene-Oligocene, sedimentation became terrestrial to lacustrine. This overall sequence shows first-order similarities with the Ulukışla Basin.

The younger stratigraphy, however, is significantly different, and is located to the north of a large fault zone that runs through the center of the Sivas Basin (**Figs 1, 3**). This fault zone consists of a series of thrusts and towards the west connects to the EFZ through a series of NE-SW striking sinistral strike-slip faults (Higgins et al., 2015; **Fig. 3**). To the east, the fault is defined by a N60°-70°E-trend with a left-lateral strike slip-component (Yilmaz & Yilmaz, 2006; Akyuz et al., 2013) that thrusts ophiolites and Cretaceous and younger sediments over folded Oligocene redbeds to the south, all along the Sivas Basin. This structure is hereafter referred to as Deliler-Tecer Fault Zone (DTFZ, **Figs 1, 3**).

In the hanging wall of the DTFZ, the northern Sivas Basin is an elongated depocenter that comprises Oligocene to Pliocene continental and marine strata including widespread Miocene evaporites overlain by continental redbeds. Salt mobility led to strong local deformation and the formation of mini-basins (Callot et al., 2014; Kergaravat et al., 2016; Pichat et al., 2016; Poisson et al., 2016; Ribes et al., 2015). In the west, Upper Miocene to recent volcanic rocks are found close to the EFZ and its connection to the Sivas fold-and-thrust belt (Cater et al., 1991; Poisson et al., 1996; Yilmaz and Yilmaz, 2006). The subhorizontal Pliocene covers parts of the Sivas Basin on both sides of the DTFZ.

3 Methods

3.1 Sampling

An extensive sample set was obtained from 21 localities, comprising of a total of 121 sites in rocks of common age from structurally coherent regions, totalling 2118 oriented paleomagnetic cores across the Upper Cretaceous to Miocene

stratigraphy of the Ulukışla and Sivas basins and sediments overlying the Tauride fold-and-thrust belt (**Figs 2, 3; Table 1,** GPS locations of all sites are supplied in the **supplementary information**). All samples were collected from sedimentary rocks. Age constraints for the sampled units come from geological maps and accompanying explanatory notes (MTA, 2002). Ages were complemented – where available – by published biostratigraphic literature (Blumenthal, 1956; Oktay, 1973; Oktay, 1982; Demirtasli et al., 1984; Atabey et al., 1990; Clark and Robertson, 2005; Gürer et al., 2016); . In a few cases, we obtained new nannofossil biostratigraphy (details supplied in the **supplementary information**). Paleomagnetic samples were collected from marine sediments (limestones, marls, and turbiditic sandstones) of Late Cretaceous to Middle Eocene as well as Miocene age, and continental clastic rocks of Oligocene and Miocene age. The samples were collected by drilling standard cores (25 mm Ø) with a gasoline-powered, water-cooled drill. Cores were oriented using a magnetic compass, and drilling orientation as well as bedding plane were corrected for the local declination of 5°E. We always sampled over a sufficiently long interval (10-30 m) per site, enough to sample paleosecular variation (PSV). In the laboratory, the cores were cut into specimens of 22 mm length using a double-blade circular saw.

3.2 Rock magnetism

Thermomagnetic analyses to determine the nature of magnetic carriers were performed on representative samples for each of the 121 sites, using a horizontal translation-type Curie Balance with cycling applied magnetic field, usually 150-300 mT (Mullender et al., 1993). Depending on the magnetic intensity of the sample, 30-100 mg of finely-crushed rock material per site was measured in a quartz vial. As a rule, eight heating-cooling cycles were applied to detect magneto-mineralogical alterations during heating. We used the following temperature scheme (in °C): 20-150, 50-250, 150-350, 250-400, 300-450, 350-525, 420-580 and 500-700.

3.3 Demagnetization

Samples were subjected to progressive stepwise demagnetization using either thermal (TH) or alternating field (AF) steps, from room temperature up to a maximum of 680°C, and a maximum field of 100mT respectively. To more efficiently separate secondary and primary components by AF demagnetization, specimens were heated to 150°C to remove possible viscous or present-day field overprints caused by weathering, and to reduce the coercivities of the secondary overprint in the natural remanent magnetization (NRM) (Van Velzen and Zijderveld, 1995). Temperatures ranging 20-680°C with increments of 20–50°C were applied to thermally demagnetize the samples in a shielded ASC TD48-SC oven. The NRM after each step was measured on a horizontal 2G DC SQUID cryogenic magnetometer (noise level $3 \times 10^{-12} Am^2$). Demagnetization steps ranging 5–100 mT with field steps of 3-10 mT were applied for AF demagnetization, performed on an in-house developed, robot assisted and fully automated 2G DC SQUID cryogenic magnetometer (Mullender et al., 2016).

3.4 Directional interpretation and statistical treatment

Paleomagnetic interpretations and statistical analyses were carried out using the platform independent portal Paleomagnetism.org (Koymans et al., 2016). All data, interpretations and statistics of this study are provided in file formats that can be imported into the portal. Stepwise demagnetization of the NRM is displayed in orthogonal vector diagrams (Zijderveld, 1967). Characteristic remanent magnetization (ChRM) directions were interpreted using principal components analysis (PCA) following an eigenvector approach (Kirschvink, 1980). Great circle analysis following McFadden and McElhinny (1988) was performed if components were not entirely resolved upon demagnetization, or became viscous or spurious at higher temperatures or coercivities. Mean directions were determined using Fisher (1953) statistics applied on virtual geomagnetic poles (VGPs) and errors in declination (ΔD_x) and inclination (ΔI_x) were calculated following Butler

(1992). We applied the reliability criteria of Deenen et al. (2011, 2014) by determining A_{95} of the VGP distribution, and calculate the n-dependent values of A_{95min} and A_{95max}: values plotting within this envelope can be explained by paleosecular variation (PSV) whilst values outside the envelope may indicate sources of enhanced scatter ($A_{95}>A_{95max}$), or under-representation of PSV ($A_{95}<A_{95min}$) e.g. due to remagnetization. To test the origin of the ChRM, field tests (reversal-test, fold-test) were performed where possible (Tauxe and Watson, 1994; Tauxe, 2010, **Fig. 7**). A fixed 45° cut-off was applied to the VGP distributions on site and locality level (Johnson et al., 2008; Deenen et al., 2011). Using these tests, we establish whether the locality carries a primary or secondary magnetization. In the discussion section, we assess the reliability and consistency of our paleomagnetic results and evaluate the tectonic implications..

3.5 Compilation of previous paleomagnetic results

We have compiled published paleomagnetic data from the Taurides, Kırşehir Block, and Pontides previously used to infer rotation patterns in Central Anatolia. This paleomagnetic database is provided in the Supplementary Information and in a Paleomagnetism.org compatible format. Literature references are provided in the description of the supplementary information. All sites are given in tectonic coordinates (i.e., corrected for bedding tilt) where possible. All paleomagnetic directions were converted to normal polarity. The database was built following selection criteria listed in Li et al. (2017). Because the paleomagnetic community does not normally publish their original data, but only the statistical parameters (Dec, Inc, N, k) of the data set, we have created parametrically sampled data sets for each site to facilitate averaging directions rather than means (see Deenen et al., 2011). Since the average directions in our compilation are based on parametric sampling, they may differ somewhat from the published ones. Locality averages for the segments of the Pontide orocline, the Kırşehir Block, and the Eastern Taurides based on these literature data are provided in **Table 1**.

4 Results

4.1 Rock magnetism

Most samples showed decreasing magnetization up to temperatures of 550-580°C, indicative for (Ti-poor) magnetite. Often, oxidation of pyrite upon thermal demagnetization forms magnetite around 400°C (Passier et al., 2001) leading to spurious demagnetization behaviour at higher temperatures. Occasionally, the presence of hematite is seen by the removal of the magnetization at temperatures as high as 680°C. These results are consistent with Curie Balance measurements, of which nine representative results are shown in **Fig. 4**. The following patterns were observed in thermomagnetic curves, which aided our demagnetization strategy, whereby hematite-bearing samples were preferably TH-demagnetized and pyrite bearing samples were AF-demagnetized. Near continuous, non-reversible alteration with increasing temperature was recorded by some light-red colored limestones and continental red siltstones or beige sandstones, showing an inflection around 350°C interpreted as inversion of maghemite into hematite (Dankers and others, 1978) and finally to magnetite at ~580°C (**Fig. 4b,h**). The presence of hematite in some red siltstones is evident from a residual magnetic signal up to 680°C (**Fig. 4e, e**). The cooling curves for these samples is below the heating curves, indicating oxidation of maghemite/magnetite, likely to hematite which has a lower spontaneous magnetization. The presence of pyrite is evident in a number of marls and limestones, where the increase in the magnetization at 390-420°C indicates that pyrite transforms to magnetite producing an intensity maximum at 480-500°C. Above 500°C, the newly formed magnetite is subsequently demagnetized or oxidized at 580°C (Fig. 4a, d, g). The cooling curves below 400°C are higher than the heating curves because of this newly formed magnetite which causes the spurious demagnetization

behaviour at temperatures above 400°C. Pyrite is not always present in the marls, as is evident from marly samples that show a continuous decay until ~580°C, indicating (T-poor) magnetite only (Fig. 4c,f,i). Sometimes the amount of magnetite is very small and the Curie curve shows a mostly paramagnetic shape (Fig. 4c,i). Nevertheless, some magnetite must have been present since the cooling curve is lower than the heating curve because of demagnetization/oxidation of the magnetite.

4.2 Demagnetization

Samples with magnetite-hosted magnetizations showed decreasing magnetization up to 550-580°C, or fields of 60-100mT. Hematite-bearing samples required higher temperatures up to 680°C. Generally, low temperature/low coercivity overprints were minor and easily removed at low temperatures (100-150°C) or low alternating fields (10-15 mT); where this was not the case, we used great circles and if possible determined great circle solutions (McFadden and McElhinny, 1988). Many samples and sites yielded no reliable paleomagnetic results and were discarded from further analysis. Below we discuss per locality the reason for discarding them. Typical causes are too low intensities, alteration upon heating and subsequent erratic magnetization behaviour, or a component that, in geographic coordinates, cannot be distinguished from a recent field overprint, *in casu* a geocentric axial dipole (GAD) direction for the locality. In interpreting the demagnetization diagrams, we did not rely on criteria for the maximum angular deviation (MAD, Kirschvink, 1980), because this cannot be justified from a statistical standpoint and depends on anchoring or not anchoring to the origin (Heslop and Roberts, 2016). In almost all cases, anchoring produces an artificially low uncertainty estimation (MAD) compared to an unanchored fit; this is inherent in the method used in the PCA analysis. In our interpretations, common sense and consistency of results dictated whether or not to anchor. Although the criteria to anchor or not to anchor have very recently been placed on a firm statistical footing by Bayesian model selection (Heslop and Roberts, 2016), this has not been implemented (yet) in the paleomagnetism.org online tool.

In determining the means per locality, we averaged all individual directions of the sites of that locality. We therefore break with paleomagnetic tradition to average the site means per locality, although these are given in **Table 1**. Site means are unit vectors irrespective of the number of samples per site, and therefore site mean cones of confidence (A95) and dispersion (K) are not propagated. By taking all site directions together, sites with more samples have, naturally, more weight. Since we use the Deenen et al., 2014, 2011 criteria, this approach is warranted because the range of acceptable A95 is N-dependent, contrary to the traditional criteria (e.g. Van der Voo, 1990; see the discussion and **Fig. 3** in Deenen et al., 2011. A95 should fall within the $A95_{min}$-$A95_{max}$ envelope, which becomes stricter ('narrower') with increasing N. The estimate of dispersion (K) of the distribution, however, is largely independent of N (for N sufficiently large, say N>10) and for increasing N becomes an increasingly better estimate for the true dispersion (κ) of the distribution.

4.3 Paleomagnetic results

Below, we describe the paleomagnetic directions obtained from each of our 21 localities. Results are summarized in **Table 1** and locality averages are illustrated in **Figs. 2 and 3**. All demagnetization diagrams per site are provided in the online supplementary information as *site*.dir files that can be imported into Paleomagnetism.org, representative examples for most localities are shown (**Fig. 5**). Statistical analysis was first performed on a per site basis (**Table 1**), whereby outliers were omitted (but are listed in **Table 1** and in the provided Paleomagnetism.org *locality*.pmag files). Subsequently, individual directions from the 21 localities were grouped and averaged (**Figs. 2, 3, 6; Table 1**). Locality averages were calculated using individual sample directions, such that large sites (large number of samples) have a larger statistical weight

than smaller ones, following procedures in (Deenen et al., 2014, 2011). Locality results are shown as equal area projections of ChRM directions and their means before and after tectonic correction (**Fig. 6, Table 1**). All locality results are provided in the online supplementary information and can be visualized and used in Paleomagnetism.org.

4.3.1 Ulukışla Basin

Within the Ulukışla Basin, we collected ~1200 samples from 49 sites, creating 13 localities consisting of Upper Cretaceous to Upper Miocene rocks (**Figs. 2; Table 1**). Here, we describe these localities from stratigraphically old to young.

Around *Alihoca*, in the south of the basin (**Fig. 2**), we collected four sites in Upper Cretaceous red hemipelagic limestones (AL1, AR2) and from blue limestones (AL3, 4) (Alihoca-1 locality). In addition, we collected one site (AL2) from Upper Paleocene silty marls (Alihoca-2 locality). An overprint in the red limestones was removed at temperatures of ~200°C, demagnetization at higher temperatures up to ~450-500°C showed a decay trending towards the origin (**Fig. 5a,b**), at temperatures above 500°C demagnetization behaviour becomes erratic. AF-demagnetization leads to great circle trajectories and incomplete demagnetization (**Fig. 5c**), but subsequent thermal demagnetization leads to a decay trending towards the origin and was used for ChRM direction interpretation (**Fig. 5d**). We interpret that the ChRM is mainly carried by (pigmentary) hematite. The blue limestones yielded directions in geographic coordinates (AL4) coinciding with the recent field component, or erratic demagnetization behaviour due to very low intensities (AL3); both sites were discarded. Sites AL1 (reversed) and AR2 (normal) do not give a positive reversal-test, and an optimal clustering of their directions at 130% unfolding (**Fig. 7a**) provides an indeterminate (but not negative) fold-test. Both sites give A95 values that are just above A95$_{min}$, showing that they may be explained by PSV, but only barely. The Paleocene site (AL2) yielded mainly great circle trajectories for AF fields up to 40mT, and displayed gyroremanence at higher coercivities (Dankers and Zijderveld, 1981). The set points derived from thermal demagnetization showed a strongly rotated reversed field. The A95 of AL2 lies within the A95$_{min-max}$ envelope. The Alihoca locality consistently shows large rotations as much as 85° ccw (**Figs 2, 6a,b**)

The Ardıçlı locality was sampled in two sites (AR1, AR3) along a road section along the canyon to Ardıçlı village in the southeast of the Ulukışla Basin (**Fig. 2**). The lithology is a dark grey sandy-silty limestone of Campanian-Maastrichtian age. A recent component was resolved at temperatures up to ~200°C and fields of ~50 mT. In most cases, linear decay towards the origin occurred at temperatures up to ~420°C (**Fig. 5e**) suggesting an iron sulphide as carrier of the magnetization. AF-demagnetization does fully demagnetize the NRM, but at fields of 60-100 mT the direction is indistinguishable from thermal demagnetization (**Fig. 5f**). The thermal and AF behaviour is consistent with the presence of fine-grained pyrrhotite which has very high coercivities (Dekkers, 1988). A total of 12 (out of 34) samples gave noisy demagnetization data from which no ChRM was interpreted. The two sites share the same bedding and a fold-test is thus not possible. The direction in tectonic coordinates would suggest a vertical axis rotation of 45.2±2.8°cw. We note, however, that A95 (2.7) is lower than the A95$_{min}$ (3.5), indicating under-sampling of PSV. This may suggest that the magnetization was acquired in a time period that was too short to fully represent PSV, generally thought to average on a ten to hundred thousand year timescale (e.g., Deenen et al., 2011, and references therein). Because both sites were collected from several tens of meters of fine-grained sediments, which likely covers a sufficiently long time interval, such undersampling may indicate remagnetization. We further note that the tilt-corrected inclination of ~30° is considerably lower than the inclination expected for Eurasia in the Late Cretaceous-Paleogene (ranging 50-55°, with an error of ±3°). Admittedly, the lower inclination may result from compaction-induced inclination shallowing (by more than 20°), but the observation that the A95 is too low to represent

PSV points to remagnetization (and hence no inclination error), we consider the inclination of ~45° in geographic coordinates is close to the expected inclination for the plate against which the Anatolian collage accreted in the Cretaceous to Paleogene, which would be consistent with a post-tilt remagnetization. In any case, the locality would indicate a major clockwise rotation, ~45° since the Late Cretaceous-Paleogene if not remagnetized, or ~80° following post-tilt remagnetization (**Fig. 6c, Table 1**).

The *Bekçili* locality consists of six sites collected from uppermost Cretaceous to Upper Paleocene marls and interbedded turbiditic sandstones (Çamardı Formation) in the northern part of the Ulukışla Basin (**Fig. 2**), between the villages of Bekçili and Üskül. A recent component is generally removed at 15 mT or ~200-250°C. Subsequently, the component trending towards to the origin between 20 and 60 mT or 250 and 560°C is interpreted as the ChRM (**Fig. 5g,h**) likely carried by magnetite. The A95 of the mean lies within the A95$_{min-max}$ envelope. In addition, the locality yields a positive fold-test (**Fig. 7b**). The Bekçili locality therefore provides a well-defined rotation of 35.4±2.9°ccw (**Figs 2, 6d**, **Table 1**).

The *Kızılkapı* locality is based on five sites sampled in Upper Paleocene marls and siltstones in the north of the basin between Kızılkapı and Postallı villages (**Fig. 2**). A recent component is generally removed at 20 mT or ~220-240°C. A component trending towards the origin between 20 and 50 mT or 275 and 450°C is interpreted as the ChRM, likely carried by magnetite. At higher temperatures, the magnetization becomes erratic because of the oxidation of pyrite. Site PC3 provided only erratic demagnetization behaviour and was discarded. Site PC1 yielded an inconsistent direction in both geographic and tectonic coordinates (D/I = ~52/-47° and 357/-65°, respectively), and was discarded from further analysis. The remaining sites CP1, PC2, and PC4 yield inclinations that are significantly steeper than predicted for the Eurasian reference (~64±4° vs. ~50°), whilst the in geographic coordinates the inclination if 46.5±5.7°. We therefore interpret the magnetization as post-tilt, suggesting a post-remagnetization, post-tilt rotation of 45.5±5.4° ccw. (**Figs 2, 6e**, **Table 1**).

The *Kolsuz* locality consists of two sites collected from Paleocene marine marls interbedded with volcanic rocks in the west of the basin (**Fig. 2**). A recent component is generally removed at 20 mT and ~180°C and decay towards the origin or great circle trends occur between 20 and 50 mT and 200 and ~450°C, suggesting magnetite as carrier. The two sites both yield reversed polarity directions with shallow inclinations of ~30°, both before and after tilt correction, which may be explained by compaction-induced inclination shallowing. A fold-test is positive **(Fig. 7c)**. The two sites combined yield an A95 value within the A95$_{min-max}$ envelope. The locality suggests a rotation of 24.2±7.8° ccw (**Figs 2, 6f**, **Table 1**).

The *Halkapınar* locality consists of nine sites collected from Paleocene to middle Eocene siltstones and marls in the southwest of the basin (**Fig. 2**). Site HP5 provided erratic demagnetization behaviour, while site HP4 yielded unrealistic inclinations both in geographic and in tectonic coordinates. Site KG1 provided a direction that in geographic coordinates coincides with the recent component, and in tectonic coordinates yielded a very low inclination of ~15°; we interpret the site as a recent overprint and discard it. Site YL1 provides a tightly clustered set of reversed directions decaying towards the origin at low temperatures of up to 200°C, with an A95 (4.3°) lower than A95$_{min}$ (6.3°). The inclination in geographic coordinates (-53±6°) coincides with the expected inclination for the sample locality, whereas in tectonic coordinates it is too low (-25±8°). We discard sites HP4, HP5, KG1, and YL1 (**Table 1**). Of the remaining five sites, KG2 and HP2 have normal polarity, and HP1, HP3 and HP6 have reversed polarity. A recent component direction was eliminated at temperatures of ~100-150°C and fields of 10-15 mT. The ChRM components were interpreted between 300 and 500-600°C and 15-80 mT (**Fig. 5i,j**). The primary carrier of the magnetic signal is magnetite. The fold-test shows optimal clustering at ~61-95%

unfolding (**Fig. 7d**). The Halkapınar sites come from a sedimentary sequence that shows evidence for syn-folding sedimentation: the lower part of this sequence is tilted steeper to the north than the upper part (Gürer et al., 2016), consistent with the fold-test, and we hence interpret the magnetization as primary. The A95 value is within the $A95_{min-max}$ envelope (Deenen et al., 2011). The locality thus provides a well-defined rotation, of 25.2 ±4.9 °ccw (**Figs 2, 6g**, **Table 1**).

The *Eminlik* locality was collected at four sites in Middle Eocene sandy and silty marls exposed in a syncline in the central part of the basin . A minor viscous component was removed at temperatures up to ~150°C. The ChRM of sites was interpreted largely between ~200-450°C and ~10-30mT. EM1 and EM5 show a declination and inclination indistinguishable from the recent magnetic field and were discarded. In geographic coordinates, sites EM2 and EM4 yielded both normal and reversed, antipodal directions with steep inclinations close to the recent field (~56°) and declinations indistinguishable from north and south, respectively. In tectonic coordinates, however, inclinations are unrealistically shallow (8-15°). We interpret these directions to reflect a post-tilt remagnetization of reversed and normal polarity and discard the sites. The four sites of the Eminlik locality hence did not provide a rotation estimate (**Table 1**).

The *Hasangazi* locality was collected from six sites sampled in grey sandy limestones and silty marls of Eocene age between Teknecukur and Hasangazi villages (**Fig. 2**). A minor viscous component was eliminated at temperatures up to 180°C. In geographic coordinates, three sites from this locality (HG1, GM2, and TC1) are indistinguishable from the recent field (**Table 1**), while site GM1 yielded erratic demagnetization behaviour. These four sites were discarded. For the remaining sites the components from 280-350°C or 20-60mT (TC2, , and 320°C-450°C or 20-60mT (HG2) were interpreted as the ChRM, or used to construct great circles (**Fig. 5k,l**). Sites HG2 and TC2 defining the Hasangazi locality (n=33) yielded a positive fold-test (**Fig. 7e**). The A95 value lies just below the $A95_{min}$ value (**Table 1**), which likely results from the use of great circles that seek optimal clustering. We obtain a rotation of 4.9°±2.8°cw (**Figs 2, 6h**, **Table 1**).

The *Topraktepe* locality was collected at a single site in Middle Eocene silty, dark limestones and marls in the central part of the basin (**Fig. 2**). A component up to ~180°C and 20 mT carries a recent component. Decay towards the origin until ~360°C is interpreted as a magnetization carried by iron sulfides, and erratic behaviour above 390-420°C is interpreted as the breakdown of pyrite into magnetite (**Fig. 4d**). The ChRM was interpreted from the linearly decaying component between ~200-350°C and ~25-40mT (**Fig. 5m,n**). The mean yields an A95 value within the $A95_{min-max}$ envelope. The inclination in geographic coordinates is lower (~27°) than in tectonic coordinates (~45°). We interpret the direction as primary, and the locality suggests a rotation of 44.5±4.1° ccw (**Figs 2, 6i**, **Table 1**).

The *Aktopra*k locality contains four sites sampled in Chattian (Upper Oligocene) continental brown and red silt and sandstones exposed in the Aktoprak syncline in the southwest of the basin. Curie balance measurements (**Fig. 4b**) identify magnetite as the main magnetic carrier. Site AT1 yielded erratic demagnetization behaviour and site AT4 yielded an average direction indistinguishable from a recent component in geographic coordinates (**Table 1**). Site AT2 did not yield components linearly decaying towards the origin, while great circles do not show a common intersection. Hence, these three sites were discarded. Site AT3 provided a component trending towards the origin, or defining great circle trajectories, between 200 and 570°C and 20-60 mT (**Fig. 5o,p**). This site suggests a rotation of 24.5±10.1°. Meijers et al. (2016) reported paleomagnetic data from the same stratigraphy based on a much larger dataset of n>120 directions that is similar to our result from AT3. Combining these results, whereby we parametrically sampled the Meijers et al. (2016) dataset, yields a

dataset with an A95 value within the A95$_{min-max}$ envelope, with a mean direction suggesting a rotation of 33.7±3.8°ccw (**Figs 2, 6j**, **Table 1**).

The *Postallı* locality is based on two sites (CP2 and CP3) sampled in red continental sandstones and siltstones, and a light-colored tuffaceous sandstone, respectively. Both sites are of (Upper?) Miocene age and are located in the northern part of the basin, north of Postallı village and dam (**Fig. 2**). In both sites a recent overprint is removed at emperatures of ~180°C. The main magnetic carrier of samples in site CP2 seems to be magnetite since the component decaying to the origin and interpreted as ChRM lies between 180°C and 500-580°C (**Fig. 5q**). However, AF-demagnetization shows a small or virtually no decrease of the NRM, which suggest a high-coercive magnetic mineral. Therefore, the most likely carrier that explains both thermal and AF behaviour is pigmentary hematite. Although AF-demagnetization did not lead to full demagnetization, components clustering - or slightly decaying towards the origin – between 25 and 60 mT were interpreted as the ChRM (**Fig. 5r**), and are consistent with the thermal demagnetizations. Site CP2 contains reversed directions. In geographic coordinates, the inclination is steep (68.6±9.0°), and becomes shallower (43.3±12.0°) in tectonic coordinates. Site CP3 hosts a component that was interpreted as ChRM between ~210-430°C and ~25-60 mT, likely carried by magnetite. This site contains both normal and reversed polarities, but we have insufficient samples for a meaningful reversal-test. The fold-test is indeterminate (maximal clustering between ~50 and 150% unfolding). A95 falls within the A95$_{min-max}$ envelope. The locality suggests a vertical axis rotation of 17.7 ± 5. 4°ccw (**Figs 2, 6k**, **Table 1**).

The *Burç* locality contains one site sampled in Upper(?) Miocene lacustrine sandstones and silts in the northeast of the basin, south of Çamardı (**Fig. 2**). This site only provided erratic demagnetization behaviour, from which no consistent ChRM component was interpreted. Hence, this locality was discarded from further analysis **(Table 1)**.

The *Hacıbekirli* locality contains one site sampled in Upper Miocene terrestrial sandstones and silts in the southwestern part of the basin (**Fig. 2**). A recent overprint is removed at temperatures of ~150°C. Components decaying towards the origin between 10 and 30 mT, and 150-350°C were interpreted as the ChRM. The site yields a reversed magnetization with a tight clustering of interpreted ChRM directions (A95 = 3.0 < A95$_{min}$=3.8), indicating remagnetization. This is supported by the direction in geographic coordinates (~182/-53°) with an inclination close to the inclination of the recent field, whereas in tectonic coordinates a direction of 165/-34° yields a much lower inclination, which would suggest major inclination shallowing (**Table 1**). In absence of positive field tests, we refrain from interpreting this direction as primary even though the rotation in tectonic coordinates (15° ccw) would be similar to that from Postallı (18° ccw) (**Figs 2, Fig. 6l**, **Table 1**).

Finally, we calculated an average paleomagnetic direction for the Upper Miocene to Pliocene volcanic rocks of *Cappadocia* overlying the AAB Block by combining lava sites previously published by Çinku et al. (2016); Piper et al. (2002, 2013); Platzman et al. (1998). These yield a mean (n=77) with an A95 (2.8) within the A95$_{min-max}$ envelope (2.1, 5.3). These data suggest a vertical axis rotation of 6.5±3.3°ccw (**Fig. 1; Table 1**).

4.3.2 Tauride fold-and-thrust belt and overlying basins

115 samples from three localities (Berendi, Aladağ, Gürün) consisting of 11 sites were sampled in the Eocene to Miocene stratigraphy of the sediments overlying the Taurides fold-and-thrust belt (**Figs. 2, 3**; **Table 1**). In addition, one locality (Sariz) with 4 sites and 63 samples was sampled from folded and thrusted Late Cretaceous-Eocene limestones within the eastern

Tauride fold-and-thrust belt. The maps (**Fig. 2,3**) show the average declination of each locality with its associated ΔD_x, whereby all directions were calculated into normal polarity.

The *Berendi* locality is based on six sites sampled from shallow marine nodular limestones overlying the Tauride fold-and-thrust belt to southwest of the Ulukışla Basin (**Fig. 2**). We obtained calcareous nannofossils from this locality (see supplementary information), showing a Thanetian (Late Paleocene) to Ypresian (Early Eocene) age. Site BR5 gives a direction indistinguishable from a recent component. while site BR6 yielded erratic demagnetization behaviour; both sites were discarded. From sites BR1-4, a low temperature but consistent component with reversed polarity was removed between 100 and 250-400°C, or between 15 and50-80 mT, and was interpreted as the ChRM (**Fig. 5s,t**), or defined by great circles. A fold-test on sites BR1-4 is clearly negative (**Fig. 7f**), implying a post-folding magnetization. The remagnetized direction in geographic coordinates has a declination of 343.1±6.2°, suggesting a post-folding rotation of 16.9°± 6.2° ccw (**Figs 2, 6m**, **Table 1**).

The *Alada*ğ locality is based on four sites sampled in folded Oligocene continental red sandstones and silts of the Karsantı Basin overlying the Taurides (Ünlügenç et al., 2015) near Aladağ village east of the EFZ (**Fig. 2**). The Lower Miocene of the Adana Basin (**Figs 1, 2**) unconformably overlying the Karsantı Basin is not folded. Sites AD1 and AD3 did not result in paleomagnetically meaningful results and were discarded. The magnetisation of sites AD4 and AD5 is primarily carried by iron sulfides, most likely pyrrhotite, because the ChRM is generally interpreted between 10-70mT, and between low temperatures of 150-300°C (**Fig. 5u,v**). Sites AD4 and AD5 yield a negative fold-test (**Fig. 7g**) showing that they carry a post-tilt magnetization acquired sometime after the Oligocene. This is further suggested by the shallow inclinations upon tectonic correction (~30° compared to ~50° in geographic coordinates). The combination of these two sites yields a declination in geographic coordinates of 343.4±7.3°, suggesting a ccw rotation of 16.6±7.3 (**Figs 2, 6n, Table 1**), with an ill-defined but post-folding age.

The *Sarız* locality consists of four sites, one in Upper Cretaceous and three in Eocene limestones sampled in the eastern Tauride fold-and-thrust belt to the north of Pınarbaşı (**Fig. 3**). In all sites, a recent component is removed at temperatures up to 180°C, or up to ~25mT, followed by erratic demagnetization behaviour. The Sarız locality yielded therefore no reliable directions and was discarded (**Table 1**).

The *Gürün* locality was sampled at one site in Miocene mudstones overlying the Eastern Taurides (**Fig. 3**). A recent component was removed at temperatures of 180°C. A component trending towards the origin was isolated between ~200 and 350-450°C and was interpreted as the ChRM, whereas AF-demagnetization did not yield paleomagnetically meaningful interpretations. In tectonic coordinates, all interpreted samples show a reverse polarity, which results in an average declination of 163.9±10.9° after tectonic correction, constraining a rotation of 16.1°±10.9° ccw (**Figs 3, 6o**, **Table 1**). No field tests can be applied to this site (SS10) and we cannot firmly conclude that this site carries a primary magnetization. In geographic coordinates, however, the declination is 146.9±12° (**Table 1**), suggesting a ccw rotation of ~33°.

4.3.3 Sivas Basin

Within the Sivas Basin, we collected ~900 samples from in total 51 sites defining 12 localities consisting of Paleocene to Upper Miocene rocks of the Sivas Basin (**Fig. 3; Table 1**). Additionally, several published magnetostratigraphic sites from

the western part of the basin were re-interpreted (Krijgsman et al., 1996; Langereis et al., 1990). One locality of three sites was sampled on the Kırşehir Block, northwest of the basin.

The *Ulaş* locality comprises nine sites from Paleocene-Eocene marls around Ulaş in the central west part of the region, ~30 km south of Sivas city (**Fig. 3**). Most sites of this locality provided either a low-temperature recent component or no results, and we discarded sites SS11, SS18, SS21 SS30 and SS31 were discarded. The remaining sites SS17, SS19, SS20 and SS29 show in most cases a recent component that is easily removed at 15mT or 180°C. ChRM components were interpreted between 10-70 mT and 250-580°C (**Fig. 5w**) and yielded well defined reversed directions that are very similar in geographic coordinates (**Table 1**). The fold-test of these sites is clearly negative (**Fig. 7h**), and the magnetisation has been acquired after folding. The declination in geographic coordinates (8.8 ± 5.3°) (**Figs 3, 6p**, **Table 1**) shows a minor cw rotation since remagnetization.

The *Akkışla* locality comprises eight sites of Eocene age in the southwest of the basin, unconformably overlying Afyon Zone metamorphic rocks east of Akkışla (**Fig. 3**). All sites were sampled from marls. Two sites (SS1, SS25) have a reversed and six have a normal polarity. Site SS4 gave a direction indistinguishable from a recent component in geographic coordinates and was discarded. In the remaining 7 sites a recent component overprint is removed at ~180°C or 10-15 mT. Components trending towards the origin were interpreted as the ChRM between a range of ~12-60 mT and 180-500°C (**Fig. 5x,y**) and are likely carried by magnetite. The A95 of the mean lies within the A95$_{min-max}$ envelope. The remaining sites yield a positive fold-test (**Fig. 7i**) and the locality mean yields a declination suggesting a rotation of 26.4 ± 3.4°ccw (**Figs 3, 6q**, **Table 1**).

The *Gürlevik* locality was sampled at five sites from Eocene marls north of Gürlevik mountain, between Sincan and Zara in the central southern part of the basin (**Fig. 3**). Sites SS36, SS43 and SS45 gave no results and were discarded. The magnetisation of the remaining sites SS3 and SS44 is primarily carried by magnetite, with the ChRM interpreted generally between 150-370°C and 20-65 mT. The two sites SS33 and SS44 give a positive fold-test (**Fig. 7j**) and have an A95 value within the A95$_{min-max}$ envelope. The declination shows a rotation of 19.8±9.5°cw in tectonic coordinates (**Figs 3, 6r**, **Table 1**).

The *Güllük* locality was sampled at five sites from Upper Eocene to Oligocene red sandstones and siltstones in the central part and north of the study area, and on the northern flank of Tecer mountain (**Fig. 3**). The magnetisation of these sites is primarily carried by magnetite, with the ChRM interpreted between generally between 100-300°C and 10-60 mT. The five sites provided generally high magnetic intensities with either components linearly decaying towards the origin, or, in most cases, well-defined great circles. Those great circles define well-clustered intersections from which sample directions were estimated. Each of the five sites yielded a well-defined average paleomagnetic direction, but these five directions are strongly scattered. This may either reflect strong local rotations – which is unlikely given the absence of mini-basins or major faults within this locality. More likely, some of these sites may have been remagnetized by lightning, which would be consistent with their high intensities. Sites SS32 and SS52 give anomalously low inclinations <15° and site SS53 gives declination suggesting a rotation of almost 100° derived from great-circle analyses only. Sites SS51 and SS54, on the other hand, give a positive fold-test (**Fig. 7k**). These two sites suggest a rotation of 37.6 ± 10.7° ccw in tectonic coordinates (**Figs 3, 6s**, **Table 1**).

The *Akdağmadeni* locality consists of three sites sampled in Eocene marls and red continental deposits overlying the easternmost part of the Kırşehir Block, northwest of the Sivas Basin (**Fig. 3**). A recent component overprint is generally

removed at fields of 15 mT and temperatures of 150°C. The primary carrier of the magnetization is magnetite. The sites are characterized by low intensities and unstable demagnetization behavior. Site SS16 only gave recent directions and was discarded. Site SS14 provides mostly erratic directions, but a few samples with reversed polarity yielded an interpretable result, where the ChRM was interpreted between 20-45 mT, and 240-370°C. The interpreted directions and great circles suggest an unrealistically low inclination upon tectonic correction (-27°), compared to in geographic coordinates (~54°). We hence interpret this site to represent a post-tilt magnetization which yields a rotation of ~20° ccw in geographic coordinates. Similarly, site SS15 provided some reversed directions, but mostly great circles that yielded no consistent intersection and the site was discarded from further analysis. A fold-test of sites SS14 and SS15 was not possible. We note that the inclination of the sites in geographic coordinates is close to the one expected based on the European APWP, whereas in tectonic coordinates, the inclination is very shallow (22-35°), which may indicate a post-tilt magnetization. When combined, the A95 of the mean lies within the $A95_{min-max}$ envelope. In tectonic coordinates, the locality yields a declination suggesting ~10°ccw rotation, in geographic coordinates, the declination would suggest a post-tilt 15°ccw rotation (**Figs 3, 6t**, **Table 1**).

The *Sincan* locality is based on one site collected in the corridor of red Oligocene siltstones and sandstones between north of Kangal and Divriği towns (**Fig. 3**). The primary carrier in this site (SS34) is magnetite. A recent component was eliminated at temperatures of ~180°C and fields of 10-15 mT (**Fig. 5z, aa**). The ChRM was interpreted between temperatures of 200-580°C and fields of 20-60 mT. The directions obtained from well-defined components trending towards the origin yields a declination of ~304.2 ± 9.0° and an inclination of 47.8 ± 9.3° in geographic coordinates, and in tectonic coordinates a declination of 277.5 ± 6.6° and a shallow inclination of 25.7 ± 11.0°. This shallow inclination may indicate that this locality acquired its magnetization after folding. We conservatively estimate a post-folding rotation of 55.8 ± 9.0°ccw (**Figs 3, 6u**, **Table 1**).

The *Yeniköy* locality consists of six sites sampled in Oligocene continental redbeds (fluvial and lacustrine siltstones and sandstones) in the southwestern part of the greater Sivas Basin, approximately 20 km south of Şarkışla (**Fig. 3**). In addition, samples from 102 levels were collected from a 800 m long section of redbeds of the Yeniköy locality by Krijgsman et al. (1996). We have reinterpreted their data for rotation analysis. Almost all new sites of this locality gave a direction in geographic coordinates that is close to a recent component. Samples from the remaining site SS58 yielded a ChRM likely carried by hematite considering the temperature needed to fully remove the NRM, in accordance with the lithology (redbeds). The A95 of the mean lies within the $A95_{min-max}$ envelope. The combined Yeniköy section and SS58 contain both normal and reversed directions. These yielded a positive reversal-test and a positive fold-test (**Fig. 7l**). The locality provides a rotation of 42.4 ± 3.2°ccw in tectonic coordinates (**Figs 3, 6v**, **Table 1**).

The *Inkonak* locality consists of an Upper Oligocene series of fluvial and lacustrine sediments sampled by Krijgsman et al. (1996) for magnetostratigraphic purposes. It was sampled ~50 km south of Sivas city (**Fig. 3**). The section is 313 m thick and consists of a regular alternation of clays, limestones and sandy deposits. We reinterpreted their demagnetization diagrams for tectonic purposes. A recent component was removed at ~100°C, the ChRM was eliminated between 240-700°C. The section yielded both normal and reversed polarity directions. Although the reversal-test was not positive in tectonic coordinates owing to an 8° difference in inclination, the declinations of both groups are identical There was insufficient variation in the bedding for a meaningful fold-test. Combining the normal and reversed directions, a mean ChRM was

obtained with an inclination of 45.9 ± 5.4° and a declination of 304.0 ± 5.0°, which suggests a rotation of 56.0 ± 5.0°ccw in tectonic coordinates (**Figs 3, 6w**, **Table 1**).

The *Gemerek* locality was sampled in the western part of the basin (**Fig. 3**) and analyzed by Krijgsman et al. (1996) for magnetostratigraphic purposes and was collected from a continuous stratigraphic section of 200 m consisting of Middle Miocene (~15 Ma) fluvial/lacustrine sediments. We have re-analyzed their data. The samples show a recent component, which was removed at 100-240°C. The ChRM component was interpreted at temperatures up to 700°C. The Gemerek locality contains both normal and reversed intervals generally yielding well-defined components trending towards the origin. The normal and reversed directions yield a positive reversal-test and a positive fold-test (**Fig. 7m**). The A95 of the mean lies within the A95$_{min-max}$ envelope. We therefore consider the magnetization as primary and interpret a rotation of 49.9 ± 3.8°ccw for this locality (**Figs 3, 6x**, **Table 1**).

The *Bünyan* locality consists of one site collected from white lacustrine marls of Miocene age in the west of the basin (**Fig. 3**). The samples of this site (SS24) only showed a recent overprint, and the locality was discarded from further analysis (**Table 1**).

The *Sivas* locality was sampled along road cuts on both sides of the main road to Sivas city, between Kovalı and Güllüce (**Fig. 3**). All four sites of the locality were sampled from Miocene continental redbeds made of sandstones and silts. Site SS12 yields five reversed directions based on high-temperature components trending towards the origin. In addition, the site yields 20 near-parallel great circles, causing the great circle solutions plus the 5 setpoints to create a very highly clustered average that we feel is not substantiated by the quality of the demagnetization diagrams. Hence, we only use the five directly obtained ChRM directions for our average. SS13 yielded well-defined great circles, yielding a well-defined intersection that we interpret as the ChRM. Site SS22 showed a recent overprint removed at temperatures of ~180°C and fields of 5 mT. A normal component interpreted as ChRM was found between 300-600°C, and 8-40 mT (**Fig. 5bb, cc**). The resulting direction yielded in geographic coordinates an inclination (59.1 ± 3.7°) close to the one expected for the locality, but a very shallow one (26.5 ± 5.5°) in tectonic coordinates, suggesting a post-tilt remagnetization. Site SS23 yielded two directly interpreted ChRM directions and a set of great circles with well-defined solutions providing the site average. The four sites yield an indeterminate fold-test, but the test is strongly influenced by the five directions of site SS12 which have strongly deviating declinations. Performing the fold-test only on SS13, SS22 and SS23 yields a negative fold-test (**Fig. 7n**) suggesting post-folding remagnetization. Moreover, the inclinations (53-59°) of the three sites in geographic coordinates are all coinciding with the expected one, but are significantly shallower in tectonic coordinates (27-44°). We thus suspect a remagnetization after (most of) the folding and interpret a post-remagnetization rotation of 16.3 ± 4.8° cw (**Figs 3, 6y**, **Table 1**).

The *Zara* locality consist of three sites sampled along road sections around Bulucan ~20 km south of Zara town (**Fig. 3**). Site SS37 was collected from shallow marine marls and sandstones and yielded a low-temperature, low-coercivity component coinciding with a recent overprint and was discarded. Sites SS35 and SS42 were sampled in Miocene siltstones and sandstones. Site SS35 yielded only recent overprints that passed the origin, but no single reliable setpoint (ChRM) could be determined. Similarly , site SS42 yielded only great circles with no clear intersection and was discarded (**Table 1**).

The *Kemah* locality consists of four Miocene sites sampled in sandstones and siltstones north of Kemah in the far east of the study region. Magnetite was identified as the primary magnetic carrier. A recent component was removed at 100-150°C and fields of 20 mT. Sites SS38 and SS40 yielded strong recent overprints which determined great cirlce trajectories with no clear intersection; both were discarded. Sites SS39 and SS41 yielded strong recent overprints, but these did not converge towards the origin and defined only great circles but no ChRM directions (**Fig.5ee, ff**), whereby the demagnetization diagram suggested that the polarity of the non-recent component was reversed. The great circles determined from each of these sites showed a clear intersection (**Fig. 5 gg,hh**), which we used to determine the ChRM directions of each site following the approach of McFadden and McElhinny (1988). The thus determined directions yielded a clearly negative fold-test (**Fig. 7o**). The Kemah locality thus shows a post-folding rotation of 6.7 ± 5.4° cw (**Figs 3, 6z, Table 1**).

The *Kalkar* locality consists of the Kaleköy and Karaözü sections (**Fig. 3**), which were sampled for magnetostratigraphic purposes by Langereis et al. (1990) in Upper Miocene (latest Vallesian; Sümengen et al., 1990) continental sediments. The continental sediments consist mainly of silts and brown clays with occasionally thick sand layers. We reinterpreted the demagnetization diagrams for tectonic purposes. A large overprint is only removed at relatively high temperatures (above 300°C) and a final component trending towards the origin is only removed at the highest temperatures (610-650°C), pointing to maghemite and/or hematite as the main carrier of the ChRM. The Kalkar section yielded normal and reversed polarity directions that yield a positive reversal-test in geographic coordinates but a negative one in tectonic coordinates. In tectonic coordinates the mean declination (~336±6°) yields a 24 ± 6°ccw rotation, but an inclination that is much shallower (~34°) than in geographic coordinates (60°). We therefore interpret the locality as remagnetized after folding, with a rotation of 10.1±10.3° cw (**Figs 3, 6aa, Table 1**).

5 Discussion

5.1 Regional versus local rotation in the Ulukışla Basin

The sampling of the Ulukışla Basin aimed to evaluate whether there is a significant rotation difference between the basin and the southern part of Kırşehir Block. Our results show that there are variations in the declinations derived from localities across the Upper Cretaceous to Upper Miocene stratigraphy of the Ulukışla Basin (**Fig. 2, Table 1**). Because Eurasia has not significantly rotated around a vertical axis in this time interval (Torsvik et al., 2012), rotation differences found in our localities must have resulted from regional tectonics, also when results from e.g. Upper Cretaceous rocks are compared with those from e.g. Eocene rocks. In the following we will discuss the meaning of each successful locality and evaluate the regional rotation of the basin, and discuss differences in the context of the major structures within the basin.

The majority of localities, covering Paleocene to Oligocene sediments, contain primary magnetizations that display evidence for counter-clockwise rotations on the order of ~20-40°. These include from E to W the Bekçili, Topraktepe, Kolsuz, Aktoprak and Halkapınar localities. Together these localities provide an Oligocene or younger, counter-clockwise rotation of the basin of 32.3±2.2° (n=326, K=16.4) when all individual directions are averaged, or 32.2±9.0° (n=5, K=84.5) when locality results are averaged.

In the southeastern parts of the basin, localities show rotations that strongly deviate from this average. The Upper Cretaceous and Paleocene sediments of the Alihoca locality in the southeast of the basin, overlying ophiolite yielded a very large counter-clockwise rotation of ~90°. Gürer et al., (2016) showed that the southern sediments of the basin revealed phases of rapid uplift and subsequent subsidence in the Late Cretaceous. The uplift-subsidence-uplift-subsidence cycle was

interpreted as the response to the underthrusting of the continental Kırşehir Block causing forearc uplift, then the potentially oceanic intra-Tauride basin causing forearc subsidence, and finally the Afyon Zone margin of the Taurides causing renewed uplift (Gürer et al., 2016; 2017). Paleocene subsidence was then accommodated along a major normal fault that bounds the basin to the south and that exhumed the Afyon Zone (Gürer et al., 2018), exposed immediately south of the Alihoca localities. Finally, the Alihoca locality is located close to the strike-slip EFZ. The strong local rotations in the Alihoca ophiolite are likely caused by these strong tectonic motions and structures, and are not representative for the Ulukışla Basin. The Ardıçlı locality was sampled in Upper Cretaceous sediments in the immediate hanging wall of a thrust where also a series of smaller strike-slip faults are found (Gürer et al., 2016) (**Fig. 2**). This locality yielded a post-folding clockwise rotation of ~80°. The very low dispersion (k=147, A95<A95$_{min}$) suggests under-sampling of PSV and may be caused be later intrusion of mafic dykes into the Cretaceous stratigraphy of the locality. We consider also the Ardıçlı rotation result as not regionally representative. Given the strong deformation, remagnetization (Ardıçlı) and indeterminate fold-test (Alihoca), we interpret these localities to record strong local rotations. The Upper Paleocene Kızılkapı sediments yielded counter-clockwise rotations of ~45° before and clockwise rotation of ~13° after tilt correction. As discussed above, inclinations are too steep after tectonic correction while the post-folding counter-clockwise rotation agrees well with the regional pattern. This indicates a post-tilt yet still pre-rotation magnetization, but given the inferred secondary nature of the magnetization, we refrain from using this locality in computing the rotation of the Ulukışla Basin. Finally, the Hasangazi locality of Eocene age defines a minor clockwise rotation. The sampled sites lie in a tightly folded plunging syncline in the footwall of the central top south-verging thrust **(Fig. 2;** Gürer et al., 2016). Hence, we interpret this rotation, even though well-defined, as a local rotation associated with the strong local deformation.

Finally, the available paleomagnetic information from Miocene stratigraphy show a smaller rotation than the Paleocene to Oligocene localities. Our compilation of previously published paleomagnetic results from the Upper Miocene to Pliocene rocks from the Cappadocia volcanic region, sampled across a large area of the southern Kırşehir Block (Çinku et al., 2016; Piper et al., 2013, 2002b; Platzman et al., 1998) yielded a minor counter-clockwise rotation of 6±3°, suggesting significant rotations predated the Late Miocene. The poorly dated but presumed Miocene Postallı locality in the northern part of the basin suggests a counter-clockwise rotation of 17.7±5.4°, suggesting that part of the rotation may have extended into the Miocene, although the small areal coverage of the site cannot exclude a local rotation origin.

Lefebvre et al. (2013) obtained paleomagnetic data from 4 sites in Cretaceous granitoids in the southern Kırşehir Block (their Ağacören-Avanos Block, or AAB) and concluded a 28-35° counter-clockwise rotation. We have recalculated the average direction of these four sites by averaging all individual directions, which yields a counter-clockwise rotation of 28.7±2.8° (n=248, K=14.8) (**Table 1**). Comparing this number to our average from Ulukışla yields a negligible rotation difference of 3.6±3.6°, suggesting that the Ulukışla Basin and southern Kırşehir Block (the AAB of Lefebvre et al. (2013)) form one coherently rotating domain, whereby our data from the Ulukışla Basin suggest an age of rotation sometime in or after the Oligocene, younger than the Paleocene-Eocene age postulated by Lefebvre et al. (2013). This age is consistent with the age of the Savcılı Thrust Zone (STZ; Lefebvre et al., 2013; Advokaat et al., 2014; Isik et al., 2014), which bounds the southern Kırşehir-Ulukışla rotating domain to the north. This thrust zone may continue into the Kurşunludag Thrust Zone in the east (Dirik and Göncüoglu, 1996).

5.2 Relationship of rotation in the Central and Eastern Taurides with the Ulukışla Basin and the southern Kırşehir Block

No paleomagnetic data are available from the carbonates of the Taurides in the Bolkardağ mountains immediately to the south of the Ulukışla Basin (and to the east of the Berendi locality) that could test whether the Central Taurides are part of the same rotating domain. Our results from the Eocene sediments of the Berendi locality overlying the Central Taurides

shows that 17±6° ccw rotation occurred following a post-folding remagnetization. We cannot constrain the timing of the folding or the remagnetization, which may thus well have occurred anytime since the (post-)Oligocene ~30°ccw rotation of the Ulukışla Basin and the AAB. The Berendi results, however, do suggest that the Bolkardağ mountains were not part of the clockwise rotating domain documented in the west-central Taurides to the northwest of the Mut basin (Çinku et al., 2016; Kissel et al., 1993; Meijers et al., 2011). The Bolkardağ mountains are separated by a fault from the Ulukışla Basin that was previously interpreted as a major back-thrust (Blumenthal, 1956; Demirtasli et al., 1984). Gürer et al. (2016; 2017), however, showed that this fault is a folded and overturned normal fault that was sealed by Eocene sediments. Although this normal fault may have accommodated a rotation difference between the Ulukışla Basin and the Bolkar mountains during its Paleocene to Early Eocene activity, it is unlikely that it accommodated major differential rotation differences since the middle Eocene. The formation of the Bolkardağ fold in Oligocene time was associated with no more than a few kilometres of shortening, which is unlikely to have resulted in a major differential rotation. We therefore conclude that the Bolkar mountains formed a coherent part of the counter-clockwise rotating domain together with the Ulukışla Basin and the southern Kırşehir Block.

Paleomagnetic data of Cinku et al. (2016) show that immediately east of the EFZ, the amount of rotation measured in Upper Cretaceous carbonates increases slightly towards the fault. Combining all their (parametrically sampled) sites yields a declination of 318.5±3.0°, suggesting a net counter-clockwise vertical axis rotation of 41.5±3° (n=154, K=16.1) **(Fig. 1,** arrow with reference 11**)**. Farther towards the east, where the strike of the eastern Taurides changes from NE-SW to ENE-WSW, the paleomagnetic data from the Tauride units are sparse, but four sites of Kissel et al. (2003) and Cinku et al. (2016) (**Fig. 1,** arrows with references 4 and 11, Eastern Taurides locality in **Fig. 3**) from Eocene limestones yield a declination of 329.8±3.8° (n=80, K=22.3), suggesting a 30.2±3.8° ccw rotation. Our Eocene Akkışla locality immediately north of the eastern Taurides (**Fig. 3**) showed a 27.6±3.7° ccw rotation, within error identical to that of the Eastern Taurides carbonates. Together, these thus provide a rotation that is indistinguishable from the rotation obtained from the Ulukışla Basin and the southern Kırşehir Block.

The ~10° rotation difference between the Cretaceous sites close to the EFZ (**Fig. 1** arrow with reference 3; Çinku et al., 2016) and the Eocene sites towards the east may be explained in two ways. Either, they may represent a small rotation associated with drag folding along the left-lateral EFZ. Alternatively, they may indicate a ~10° rotation occurring between the Late Cretaceous and the Eocene, when the Tauride rocks were still connected to the downgoing African Plate. Between ~80 and ~50 Ma, Africa did experience a 10° ccw rotation. In absence of a detailed structural model for the eastern Taurides showing from which nappes the paleomagnetic data were obtained, and when those nappes were incorporated in the Tauride fold-and-thrust belt, we cannot determine which of these two solutions is the more likely. We interpret that the Taurides have undergone a coherent 30°ccw rotation since Oligocene time, and that the shearing along the EFZ did not lead to strong regional extra rotations.

Oligocene sediments overlying the Eastern Tauride fold-and-thrust belt in our Aladağ locality reveal a post-folding magnetization revealing a 17±7°ccw rotation. Since the timing of its remagnetization cannot be constrained and may well have occurred during the rotation phase, this sheds no light on the timing of the eastern Tauride rotation. Our Miocene site Gürün shows a counter-clockwise rotation of 16±11° (**Fig. 3, Table 1**), and the Kepezdağ and Yamadağ localities of Gürsoy et al., (2011) obtained from middle Miocene (13-15 Ma) lavas show 26±20° and 28±6° ccw, respectively (**Fig. 1**, arrows with reference 6). Taken together, those data may suggest that the eastern Tauride rotations occurred in Middle Miocene or younger time, but we note that these Miocene lavas were sampled in the close vicinity of Middle Miocene and younger left-lateral strike-slip faults (Westaway & Arger, 2001; Kaymakci et al., 2010), and may thus not be representative for the timing of regional rotation. Three sites (**Fig. 1**; arrows with references 8, 11) from middle and upper Miocene

sediments in the Adana Basin (Çinku et al., 2016; Lucifora et al., 2012) yield a declination of 354.3±3.8° (n=134, K=14.4), suggesting a minor rotation of 5.7±3.8°, suggesting a pre-middle Miocene rotation. We tentatively suggest that the regional rotation of the eastern Taurides occurred sometime between the Eocene and middle Miocene, and was further locally modified by Miocene left-lateral strike-slip faults.

5   Overall, the sense and magnitude of the Central and Eastern Tauride rotations, those obtained from the stratigraphy of the Ulukışla Basin and those previously reported from the southern part of the Kırşehir Block (Lefebvre et al., 2013), suggest that the region rotated as a more or less coherent block, which has undergone a counter-clockwise rotation of ~30°, (largely) sometime in Oligocene or Early Miocene time.

10   **5.3 Rotations in the Sivas Basin, and the boundary of the south-east Anatolian counter-clockwise rotating domain**

Our results from the Sivas Basin show that extensive sampling was required to obtain rotation patterns, as only ~30% of samples and sites yielded meaningful paleomagnetic results. This is largely caused by (true or suspected) post-folding remagnetization, particularly to the north of the Deliler-Tecer Fault Zone (DTFZ). Nevertheless, our results lead us to the following first-order interpretation of rotations in the Sivas Basin.

15   We subdivide the Sivas region into three domains (**Fig. 8**). These are 1) the area exposing Eocene and Oligocene sediments to the south of, and in the footwall of the top-to-the-south DTFZ, 2) the area exposing Paleogene sediments immediately north, and in the hangingwall of this thrust zone, and 3) the Miocene and younger sediments occupying the northernmost part of the basin. The rotations in the Oligocene corridor of the southern domain are constrained by – from E to W - the Sincan, Inkonak and Yeniköy localities (**Fig. 3**), which reveal a combined counter-clockwise rotation of 48.1±2.9° (n=191,

20   K=15.8). Also, the Middle Miocene Gemerek locality (Krijgsman et al., 1996) yielded such high rotations (49.9±3.8°, **Table 1**). Interestingly, these rotations are ~15-20° more ccw than those recorded in the Eastern Tauride fold-and-thrust belt. This difference may be interpreted in different ways. On the one hand, it may suggest that the Taurides underwent a clockwise rotation between the Eocene and Oligocene of 15-20°, followed by a 50° rotation after deposition of the middle Miocene Gemerek section. This, however, is inconsistent with the directions obtained from Oligocene sediments in the

25   Ulukışla Basin or Miocene sediments overlying the Taurides (**Fig. 2**). We thus assume that the area to the south of the DTFZ was part of the Eastern Tauride rotating domain and tentatively ascribing the excess ~15° rotation to the local deformation in the footwall of the DTFZ, e.g. introduced by a sinistral component of the fault zone as postulated by Yilmaz and Yilmaz, (2006).

A distinct break in rotation sense occurs across the DTFZ (**Figs 3, 8**), north of which rotations are variable but generally

30   clockwise, rotating as much as ~30° in the central and northern part of the basin (Gürlevik, Ulaş, Sivas, Kemah localities). Explaining the variable clockwise rotations is not straightforward, but well-documented intense deformation, in part associated with intense local salt tectonics (Kergaravat et al., 2016; Pichat et al., 2016; Poisson et al., 2016; Ribes et al., 2015) may provide an explanation. We note, however, that one Oligocene locality (Güllük) to the north of the DTFZ reveals the counter-clockwise rotations characteristic for the area to its south. Farther to the north, in the eastern Kırşehir Block,

35   or the eastern Pontides north of the North Anatolian Fault Zone, no major counter-clockwise rotations were reported. The northeastern Kırşehir Block (the AYB Block of Lefebvre et al. (2013) experienced 18.4±6.0° clockwise rotation measured in Upper Cretaceous granitoids. The eastern Pontides experienced only minor rotations since Late Cretaceous-Eocene time, and a compilation of existing data (Baydemir, 1990; Channell et al., 1996; Kissel et al., 2003; Meijers et al., 2010; Orbay and Bayburdi, 1979; van der Voo, 1968).

40   We therefore suggest that the boundary of the coherently counter-clockwise rotating domain of the Eastern Taurides most likely coincides with the Deliler-Tecer Fault Zone (DTFZ) (**Fig. 8**). Previously, Lefebvre et al. (2013) suggested that the

counter-clockwise rotation of the southern Kırşehir Block was bounded in the north along the top-to-the-south Savcılı Thrust Zone (STZ), below which deformed and folded sediments are found similar in age and facies as those below the DTFZ. Given this similarity, and the coherence in rotation direction, amount, and timing, we infer that the counter-clockwise rotating domain of central and southern Anatolia, comprising the southern Kırşehir Block, the Ulukışla Basin, the

5   Bolkar mountains, the eastern Taurides, and the southern part of the Sivas Basin, was bounded to the north by a thrust fault zone comprising the STZ in the west, and the DTFZ in the east. Using all published and new paleomagnetic sites from Cretaceous to Neogene rocks in this rotating domain, we computed an Apparent Polar Wander Path (**Fig. 9, Table 2**) for the SE Anatolian rotating block. From this APWP, it is clear that this domain rotated ~30-35° ccw relative to Eurasia, largely in Oligo-Miocene time. As mentioned above, the declination trend for the Cretaceous is parallel to Africa, confirming that the

10   Taurides in that time were still part of the African Plate.

Finally, the eastern Taurides appear to have rotated coherently with the southern Kırşehir Block and the Ulukışla Basin, but we note that they were displaced relative to the latter along the EFZ (**Fig. 8**). This fault is controlled by the eastern margin of the Kırşehir Block, and its left-lateral displacement requires that the Sivas Basin underwent 60-70 km more N-S Eocene-Early Miocene convergence than Central Anatolia. This excess convergence is likely responsible for the much stronger

15   deformation, and probably the more disperse rotation patterns, associated with the structural growth of the Sivas fold-and-thrust belt.

6 Conclusion

In this paper, we provide a large set of new paleomagnetic data from central southern and central eastern Anatolia to aid kinematic restoration of the Anatolian Orogen. We aimed to identify the timing, amount, and regional coherence of

20   rotating blocks in central and southern Anatolia. Our main findings can be summarized as follows:

1. The Ulukışla Basin underwent a regional counter-clockwise rotation of ~32.5±2.2° in Oligocene and Miocene times, comparable with the amount and sense of rotation (28-35°) previously reported for the southern part of the Kırşehir Block. This rotation phase is contemporaneous with the activity of the STZ as a contractional structure and onset of the major left-lateral EFZ, and possibly with similar structures within the eastern Taurides (e.g.

25   Malatya Fault, MFZ in **Figs** 1, 8). Deviations from this regionally consistent pattern are found in the southern and south-eastern part of the basin, where local rotations strongly deviating from this average, owing to vicinity to major tectonic structures, such as the EFZ.

2. We find ~17 counter-clockwise rotation in Eocene, but remagnetized, sedimentary rocks overlying the Central Tauride fold-and-thrust belt in the Bolkar mountains. This suggests that the Bolkar mountains were part of the

30   counter-clockwise rotating domain as opposed to clockwise rotations found in the western Central Taurides. The total amount of counter-clockwise rotation since the Eocene cannot be determined due to remagnetization, but absence of a major Oligocene or younger fault between the Ulukışla Basin and the Bolkar mountains lead us to include these in the counter-clockwise rotating south Anatolian domain.

3. Counter-clockwise rotations were previously reported from the Eastern Taurides. These show a comparable ~30°

35   ccw rotation since the Eocene. Larger ccw rotations are reported close to the EFZ, which dissects the Taurides in its central and eastern parts, and plays a major role in the growth of the Sivas fold-and-thrust belt. Our new paleomagnetic data from the Sivas fold-and-thrust belt, reveals that on average ~48° counter-clockwise rotations

can be traced into the footwall of the DTFZ. In the hanging wall of this thrust, paleomagnetic data quality is generally low, but successful sites show consistently minor (7-20°) clockwise rotations.

4. We conclude that the southern Kırşehir Block, Ulukışla Basin, Bolkar mountains, eastern Taurides, and the southern part of the Sivas Basin were part of one coherently counter-clockwise rotating domain that experienced ~30° rotation in Oligocene or earliest Miocene time. Structural constraints suggest that this domain was bounded in the north by the STZ and DTFZ and in the south by the African-Arabian trench. To the west, the boundary is diffuse and requires future study.

Author contribution

DG and DJJvH designed the study. DG, MÖ carried out the bulk of the sampling, with support from DJJvH, IC, MK, CL. IC and MK helped with acquiring paleomagnetic data. AC provided biostratigraphic constraints. CL, DG, DJJvH, MÖ interpreted the data. DG and DJJvH prepared the manuscript.

Acknowledgments

DG, DJJvH were supported by ERC-Starting Grant 306810. DJJvH acknowledges NWO Vidi grant 864.11.004. Pinar Ertepinar and Nur Güneli are thanked for field assistance and logistical support. W. Krijgsman is thanked for providing the original data files of a previously published dataset. The authors declare that they have no conflict of interest. Aral Okay, Giovanni Muttoni and two anonymous reviewers are thanked for useful comments.

References

Advokaat, E.L., van Hinsbergen, D.J.J., Kaymakci, N., Vissers, R.L.M., Hendriks, B.W.H., Kaymakcı, N., Vissers, R.L.M., Hendriks, B.W.H., 2014. Late Cretaceous extension and Palaeogene rotation-related contraction in Central Anatolia recorded in the Ayhan-Büyükkışla basin. Int. Geol. Rev. 56, 1813–1836. https://doi.org/10.1080/00206814.2014.954279

Akyuz, H.S., Ucarkus, G., Altunel, E., Dogan, B., Dikbas, A., 2013. Paleoseismological investigations on a slow-moving active fault in central Anatolia, Tecer Fault, Sivas. Ann. Geophys. 55.

Alan, I., Şahin, Ş., Bakırhan, B., 2011. Turkish Geological Map Series, Adana N33, General Directorate of Mineral Research and Exploration (MTA), Ankara.

Atabey, E., Göncüoglu, M.C., Turhan, N., 1990. Turkish Geological Map Series, Kozan M33 (J19), General Directorate of Mineral Research and Exploration (MTA), Ankara.

Barrier, E., Vrielynck, B., 2008. Palaeotectonic maps of the middle east - Middle Aptian.

Baydemir, N., 1990. Palaeomagnetism of the Eocene volcanic rocks in the eastern Black Sea region. J Earth Sci 7, 167–176.

Blumenthal, M.M., 1956. Yüksek Bolkardağın kuzey kenar bölgelerinin ve batı uzantılarının jeolojisi: (Güney Anadolu Torosları). Maden Tetkik ve Arama Enstitüsü.

Boztuğ, D., Jonckheere, R.C., Heizler, M., Ratschbacher, L., Harlavan, Y., Tichomirova, M., 2009. Timing of post-obduction granitoids from intrusion through cooling to exhumation in central Anatolia, Turkey. Tectonophysics 473, 223–233. https://doi.org/10.1016/j.tecto.2008.05.035

Boztuğ, D., Jonckheere, R.C., Heizler, M., Ratschbacher, L., Harlavan, Y., Tichomirova, M., 2009. Timing of post-obduction granitoids from intrusion through cooling to exhumation in central Anatolia, Turkey. Tectonophysics 473, 223–233.

https://doi.org/10.1016/j.tecto.2008.05.035

Butler, R.F., 1992. Paleomagnetism: Magnetic Domains to Geologic Terranes. Blackwell Scientific Publications.

Callot, J.-P., Ribes, C., Kergaravat, C., Bonnel, C., Temiz, H., Poisson, A., Vrielynck, B., Salel, J.-F., Ringenbach, J.-C., 2014. Salt tectonics in the Sivas basin (Turkey): crossing salt walls and minibasins. Bull. la Soci{é}t{é} g{é}ologique Fr. 185, 33–42.

Cater, J.M.L., Hanna, S.S., Ries, A.C., Turner, P., 1991. Tertiary evolution of the Sivas Basin, central Turkey. Tectonophysics 195, 29–46.

Çemen, I., Göncüoglu, M.C., Dirik, K., 1999. Structural evolution of the Tuzgölü basin in Central Anatolia, Turkey. J. Geol. 107, 693–706.

Channell, J.E.T., Tüysüz, O., O., B., Şengör, A.M.C., 1996. Cretaceous paleomagnetism and paleogeography of the Pontides (Turkey). Tectonics 15, 201–212.

Çinku, M.C., Hisarli, Z.M., Yılmaz, Y., Ülker, B., Kaya, N., Öksüm, E., Orbay, N., Özbey, Z.Ü.Ü.Ü., Cinku, M.C., Hisarli, Z.M., Yilmaz, Y., Ülker, B., Kaya, N., Öksüm, E., Orbay, N., Özbey, Z.Ü.Ü.Ü., 2016. The tectonic history of the Niğde-Kırşehir Massif and the Taurides since the Late Mesozoic: Paleomagnetic evidence for two-phase orogenic curvature in Central Anatolia. Tectonics 35, 772–811.

Clark, M., Robertson, A., 2005. Uppermost Cretaceous-Lower Tertiary Ulukisla Basin, south-central Turkey: Sedimentary evolution of part of a unified basin complex within an evolving Neotethyan suture zone. Sediment. Geol. 173, 15–51. https://doi.org/10.1016/j.sedgeo.2003.12.010

Clark, M., Robertson, A., 2002. The role of the Early Tertiary Ulukisla Basin, southern Turkey, in suturing of the Mesozoic Tethys ocean. J. Geol. Soc. London. 159, 673–690. https://doi.org/10.1144/0016-764902-015

Dankers, P.H.M., others, 1978. Magnetic properties of dispersed natural iron-oxides of known grain size.

Dankers, P.H.M., Zijderveld, J.D.A., 1981. Alternating field demagnetization of rocks, and the problem of gyromagnetic remanence. Earth Planet. Sci. Lett. 53, 89–92.

Deenen, M.H.L., Langereis, C.G., van Hinsbergen, D.J.J., Biggin, A.J., 2014. Erratum: Geomagnetic secular variation and the statistics of palaeomagnetic directions. Geophys. J. Int. 197, 643.

Deenen, M.H.L., Langereis, C.G., van Hinsbergen, D.J.J., Biggin, A.J., 2011. Geomagnetic secular variation and the statistics of palaeomagnetic directions. Geophys. J. Int. 186, 509–520. https://doi.org/10.1111/j.1365-246X.2011.05050.x

Dekkers, M.J., 1988. Magnetic properties of natural pyrrhotite Part I: Behaviour of initial susceptibility and saturation-magnetization-related rock-magnetic parameters in a grain-size dependent framework. Phys. Earth Planet. Inter. 52, 376–393.

Demirtasli, E., Turhan, N., Bilgin, A.Z., Selim, M., 1984. Geology of the Bolkar mountains, in: Geology of the Taurus Belt. Proceedings of the International Symposium on the Geology of the Taurus Belt, Ankara, Turkey. Mineral Resources and Exploration Institute of Turkey, Ankara. pp. 12–141.

Dirik, K., Göncüoglu, M.C., 1996. Neotectonic characteristics of central Anatolia. Int. Geol. Rev. 38, 807–817.

Dokuz, A., Aydincakir, E., Kandemir, R., Karsli, O., Siebel, W., Derman, A.S., Turan, M., 2017. Late Jurassic Magmatism and Stratigraphy in the Eastern Sakarya Zone, Turkey: Evidence for the Slab Breakoff of Paleotethyan Oceanic Lithosphere. J. Geol. 125, 1–31.

Espurt, N., Hippolyte, J.-C., Kaymakci, N., Sangu, E., 2014. Lithospheric structural control on inversion of the southern margin of the Black Sea Basin, Central Pontides, Turkey. Lithosphere 6, 26–34. https://doi.org/10.1130/l316.1

Fisher, R., 1953. Dispersion on a Sphere. Proc. R. Soc. A Math. Phys. Eng. Sci. 217, 295–305. https://doi.org/10.1098/rspa.1953.0064

Gautier, P., Bozkurt, E., Bosse, V., Hallot, E., Dirik, K., 2008. Coeval extensional shearing and lateral underflow during Late Cretaceous core complex development in the Niğde Massif, Central Anatolia, Turkey. Tectonics 27. https://doi.org/10.1029/2006TC002089

Gautier, P., Bozkurt, E., Hallot, E., Dirik, K., 2002. Dating the exhumation of a metamorphic dome: geological evidence for pre-Eocene unroofing of the Nigde Massif (Central Anatolia, Turkey). Geol. Mag. 139, 559–576. https://doi.org/10.1017/S0016756802006751

Göncüoglu, M.C., 1997. Distribution of Lower Paleozoic rocks in the Alpine terranes of Turkey. Early Paleoz. NW Gondwana 3, 13–23.

Gülyüz, E., Kaymakci, N., Meijers, M.J.M., Hinsbergen, D.J.J. Van, Lefebvre, C., Vissers, R.L.M., Hendriks, B.W.H., Peynircioglu, A.A., 2013. Tectonophysics Late Eocene evolution of the Çiçekdağı Basin (central Turkey): Syn-sedimentary compression during microcontinent – continent collision in central Anatolia. Tectonophysics 602, 286–299. https://doi.org/10.1016/j.tecto.2012.07.003

Gürer, D., Plunder, A., Kirst, F., Corfu, F., Schmid, S.M., van Hinsbergen, D.J.J., 2018. A long-lived Late Cretaceous-Early Eocene extensional province in Anatolia? Structural evidence from the Ivriz Detachment, southern central Turkey. Earth Planet. Sci. Lett. 111--124.

Gürer, D., van Hinsbergen, D.J.J., Matenco, L., Corfu, F., Cascella, A., Hinsbergen, D.J.J. van, Matenco, L., Corfu, F., Cascella, A., 2016. Kinematics of a former oceanic plate of the Neotethys revealed by deformation in the Ulukışla basin (Turkey). Tectonics 35, 2385–2416. https://doi.org/10.1002/2016TC004206

Gürsoy, H., Tatar, O., Piper, J.D.A., Koçbulut, F., Akp\inar, Z., Huang, B., Roberts, A.P., Mesci, B.L., 2011. Palaeomagnetic study of the Kepezdağ and Yamadağ volcanic complexes, central Turkey: Neogene tectonic escape and block definition in the central-east Anatolides. J. Geodyn. 51, 308–326.

Gutnic, M., Monod, O., Poisson, A., Dumont, J.-F., 1979. Géologie des Taurides occidentales (Turquie). Mémoires la Société géologique Fr. 137, 1–112.

Heslop, D., Roberts, A.P., 2016. Analyzing paleomagnetic data: to anchor or not to anchor? J. Geophys. Res. Solid Earth.

Higgins, M., Schoenbohm, L.M., Brocard, G., Kaymakci, N., Gosse, J.C., Cosca, M.A., 2015. New kinematic and geochronologic evidence for the Quaternary evolution of the Central Anatolian fault zone (CAFZ). Tectonics 34, 2118–2141.

Isik, V., 2009. The ductile shear zone in granitoid of the Central Anatolian Crystalline Complex, Turkey: Implications for the origins of the Tuzgölü basin during the Late Cretaceous extensional deformation. J. Asian Earth Sci. 34, 507–521. https://doi.org/10.1016/j.jseaes.2008.08.005

Isik, V., Lo, C.-H., Göncüoğlu, C., Demirel, S., 2008. 39 Ar/ 40 Ar Ages from the Yozgat Batholith: Preliminary Data on the Timing of Late Cretaceous Extension in the Central Anatolian Crystalline Complex, Turkey. J. Geol. 116, 510–526. https://doi.org/10.1086/590922

Isik, V., Uysal, I.T., Caglayan, A., Seyitoglu, G., 2014. The evolution of intraplate fault systems in central Turkey: Structural evidence and Ar-Ar and Rb-Sr age constraints for the Savcili Fault Zone. Tectonics 33, 1875–1899.

Jaffey, N., Robertson, A.H.F., 2001. New sedimentological and structural data from the Ecemis Fault Zone, southern Turkey: implications for its timing and offset and the Cenozoic tectonic escape of Anatolia. J. Geol. Soc. London 158, 367–378. https://doi.org/10.1144/jgs.158.2.367

Johnson, C.L., Constable, C.G., Tauxe, L., Barendregt, R., Brown, L.L., Coe, R.S., Layer, P., Mejia, V., Opdyke, N.D., Singer, B.S., others, 2008. Recent investigations of the 0--5 Ma geomagnetic field recorded by lava flows. Geochemistry, Geophys. Geosystems 9.

Kaymakci, N., Duermeijer, C.E., Langereis, C., White, S.H., Van Dijk, P.M., 2003. Palaeomagnetic evolution of the Çankiri Basin (central Anatolia, Turkey): implications for oroclinal bending due to indentation. Geol. Mag. 140, 343–355. https://doi.org/10.1017/S001675680300757X

Kaymakci, N., Inceoz, M., Ertepinar, P., Koc, a., 2010. Late Cretaceous to Recent kinematics of SE Anatolia (Turkey). Geol. Soc. London, Spec. Publ. 340, 409–435. https://doi.org/10.1144/SP340.18

Kaymakci, N., Özçelik, Y., White, S.H., Van Dijk, P.M., 2009. Tectono-stratigraphy of the Çankırı Basin: late Cretaceous to early Miocene evolution of the Neotethyan suture zone in Turkey. Geol. Soc. London, Spec. Publ. 311, 67–106.

Kergaravat, C., Ribes, C., Legeay, E., Callot, J.-P., Kavak, K.S., Ringenbach, J.-C., 2016. Minibasins and salt canopy in foreland fold-and-thrust belts: The central Sivas Basin, Turkey. Tectonics 35, 1342–1366.

Kirschvink, J.L., 1980. The least-squares line and plane and the analysis of palaeomagnetic data. Geophys. J. Int. 62, 699–718. https://doi.org/10.1111/j.1365-246X.1980.tb02601.x

Kissel, C., Averbuch, O., de Lamotte, D.F., Monod, O., Allerton, S., 1993. First paleomagnetic evidence for a post-Eocene clockwise rotation of the Western Taurides thrust belt east of the Isparta reentrant (Southwestern Turkey). Earth Planet. Sci. Lett. 117, 1–14. https://doi.org/10.1016/0012-821X(93)90113-N

Kissel, C., Lai, C., Poisson, A., Görür, N., 2003. Paleomagnetic reconstruction of the Cenozoic evolution of the Eastern Mediterranean. Tectonophysics 362, 199–217. https://doi.org/10.1016/S0040-1951(02)00638-8

Koymans, M.R., Langereis, C.G., Pastor-Galán, D., van Hinsbergen, D.J.J., 2016. Paleomagnetism. org: An online multi-platform open source environment for paleomagnetic data analysis.

Krijgsman, W., Duermeijer, C.E., Langereis, C.G., de Bruijn, H., Saraç, G., Andriessen, P.A.M., 1996. Magnetic polarity stratigraphy of late Oligocene to middle Miocene mammal-bearing continental deposits in central Anatolia (Turkey). Newsletters Stratigr. 13–29.

Langereis, C.G., Sen, S., Sümengen, M., Ünay, E., 1990. Preliminary magnetostratigraphic results of some Neogene mammal localities from Anatolia (Turkey), in: European Neogene Mammal Chronology. Springer, pp. 515–525.

Lefebvre, C., Barnhoorn, A., van Hinsbergen, D.J.J., Kaymakci, N., Vissers, R.L.M., 2011. Late Cretaceous extensional denudation along a marble detachment fault zone in the Kırşehir massif near Kaman, central Turkey. J. Struct. Geol. 33, 1220–1236. https://doi.org/10.1016/j.jsg.2011.06.002

Lefebvre, C., Kalijn Peters, M., Wehrens, P.C., Brouwer, F.M., van Roermund, H.L.M., 2015. Thermal history and extensional exhumation of a high-temperature crystalline complex (Hırkadağ Massif, Central Anatolia). Lithos 238, 156–173. https://doi.org/10.1016/j.lithos.2015.09.021

Lefebvre, C., Meijers, M.J.M., Kaymakci, N., Peynircioğlu, A., Langereis, C.G., van Hinsbergen, D.J.J., 2013. Reconstructing the geometry of central Anatolia during the late Cretaceous: Large-scale Cenozoic rotations and deformation between the Pontides and Taurides. Earth Planet. Sci. Lett. 366, 83–98. https://doi.org/10.1016/j.epsl.2013.01.003

Li, S., Advokaat, E.L., van Hinsbergen, D.J.J., Koymans, M., Deng, C., Zhu, R., 2017. Paleomagnetic constraints on the Mesozoic-Cenozoic paleolatitudinal and rotational history of Indochina and South China: Review and updated kinematic reconstruction. Earth-Science Rev.

Lucifora, S., Cifelli, F., Mattei, M., Sagnotti, L., Cosentino, D., Roberts, A.P., 2012. Inconsistent magnetic polarities in magnetite-and greigite-bearing sediments: Understanding complex magnetizations in the late Messinian in the Adana Basin (southern Turkey). Geochemistry, Geophys. Geosystems 13.

Lucifora, S., Cifelli, F., Rojay, F.B., Mattei, M., 2013. Paleomagnetic rotations in the Late Miocene sequence from the Çankırı Basin (Central Anatolia, Turkey): the role of strike-slip tectonics. Turkish J. Earth Sci. 22, 778–792.

McFadden, P.L., McElhinny, M.W., 1988. The combined analysis of remagnetization circles and direct observations in

palaeomagnetism. Earth Planet. Sci. Lett. 87, 161–172.

Meijers, M.J.M., Kaymakci, N., Van Hinsbergen, D.J.J., Langereis, C.G., Stephenson, R.A., Hippolyte, J.-C.C., 2010. Late Cretaceous to Paleocene oroclinal bending in the central Pontides (Turkey). Tectonics 29. https://doi.org/10.1029/2009TC002620

5   Meijers, M.J.M., Strauss, B.E., Özkaptan, M., Feinberg, J.M., Mulch, A., Whitney, D.L., Kaymakci, N., 2016. Age and paleoenvironmental reconstruction of partially remagnetized lacustrine sedimentary rocks (Oligocene Aktoprak basin, central Anatolia, Turkey). Geochemistry, Geophys. Geosystems 17, 914–939. https://doi.org/10.1002/2015GC006209

Meijers, M.J.M., van Hinsbergen, D.J.J., Dekkers, M.J., Altiner, D., Kaymakci, N., Langereis, C.G., 2011. Pervasive Palaeogene
10   remagnetization of the central Taurides fold-and-thrust belt (southern Turkey) and implications for rotations in the Isparta Angle. Geophys. J. Int. 184, 1090–1112.

Menant, A., Jolivet, L., Vrielynck, B., 2016. Kinematic reconstructions and magmatic evolution illuminating crustal and mantle dynamics of the eastern Mediterranean region since the late Cretaceous. Tectonophysics 675, 103–140.

Moix, P., Beccaletto, L., Kozur, H.W., Hochard, C., Rosselet, F., Stampfli, G.M., 2008. A new classification of the Turkish
15   terranes and sutures and its implication for the paleotectonic history of the region. Tectonophysics 451, 7–39. https://doi.org/10.1016/j.tecto.2007.11.044

Monod, O., 1977. Recherches géologiques dans le Taurus occidental au Sud de Beysehir (Turquie). Univ. Paris Sud, Orsay, France.

MTA, 2002. Geological map of Turkey, scale 1:500,000., Mineral Research and Exploration Institute of Turkey.

20   Mullender, T.A.T., Frederichs, T., Hilgenfeldt, C., de Groot, L. V, Fabian, K., Dekkers, M.J., 2016. Automated paleomagnetic and rock magnetic data acquisition with an in-line horizontal "2G" system. Geochemistry, Geophys. Geosystems 17, 3546–3559.

Mullender, T.A.T., Van Velzen, A.J., Dekkers, M.J., 1993. Continuous drift correction and separate identification of ferrimagnetic and paramagnetic contributions in thermomagnetic runs. Geophys. J. Int. 114, 663–672.

25   Nikishin, A.M., Okay, A.I., Tüysüz, O., Demirer, A., Amelin, N., Petrov, E., 2015. The Black Sea basins structure and history: New model based on new deep penetration regional seismic data. Part 1: Basins structure and fill. Mar. Pet. Geol. 59, 638–655. https://doi.org/10.1016/j.marpetgeo.2014.08.017

Okay, A.I., Nikishin, A.M., 2015. Tectonic evolution of the southern margin of Laurasia in the Black Sea region. Int. Geol. Rev. 1–26. https://doi.org/10.1080/00206814.2015.1010609

30   Okay, A.I., Tüysüz, O., 1999. Tethyan sutures of northern Turkey. Geol. Soc. London, Spec. Publ. 156, 475–515. https://doi.org/10.1144/GSL.SP.1999.156.01.22

Okay, a. I., Sunal, G., Tüysüz, O., Sherlock, S., Keskin, M., Kylander-Clark, a. R.C., 2014. Low-pressure-high-temperature metamorphism during extension in a Jurassic magmatic arc, Central Pontides, Turkey. J. Metamorph. Geol. 32, 49–69. https://doi.org/10.1111/jmg.12058

35   Oktay, F.Y., 1982. Stratigraphy and geological history of Ulukısla and its surroundings. Bull. Turkish Geol. Soc. 25, 15–23.

Oktay, F.Y., 1973. Sedimentary and tectonic history of the Ulukisla area, southern Turkey. University of London.

Orbay, N., Bayburdi, A., 1979. Palaeomagnetism of dykes and tuffs from the Mesudiye region and rotation of Turkey. Geophys. J. Int. 59, 437–444.

Özdamar, Ş., Billor, M.Z., Sunal, G., Esenli, F., Roden, M.F., 2013. First U-Pb SHRIMP zircon and 40Ar/39Ar ages of
40   metarhyolites from the Afyon-Bolkardag Zone, SW Turkey: Implications for the rifting and closure of the Neo-Tethys. Gondwana Res. 24, 377–391. https://doi.org/10.1016/j.gr.2012.10.006

Özgül, N., 1984. Stratigraphy and tectonic evolution of the Central Taurides. Geol. Taurus belt 77–90.

Parlak, O., Colakoglu, A., Donmez, C., Sayak, H., Yildirim, N., Turkel, A., Odabasi, I., 2012. Geochemistry and tectonic significance of ophiolites along the Izmir-Ankara-Erzincan Suture Zone in northeastern Anatolia. Geol. Soc. London, Spec. Publ. 372, 75–105. https://doi.org/10.1144/SP372.7

Passier, H.F., De Lange, G.J., Dekkers, M.J., 2001. Magnetic properties and geochemistry of the active oxidation front and the youngest sapropel in the eastern Mediterranean Sea. Geophys. J. Int. 145, 604–614.

Pichat, A., Hoareau, G., Callot, J.-P., Ringenbach, J.-C., 2016. Diagenesis of Oligocene continental sandstones in salt-walled mini-basins—Sivas Basin, Turkey. Sediment. Geol. 339, 13–31.

Piper, J.D.A., Guersoy, H. l, Tatar, O., Isseven, T., Kocyigit, A. l, 2002a. Palaeomagnetic evidence for the Gondwanian origin of the Taurides and rotation of the Isparta Angle, southern Turkey. Geol. J. 37, 317–336.

Piper, J.D.A., Gürsoy, H., Tatar, O., 2002b. Palaeomagnetism and magnetic properties of the Cappadocian ignimbrite succession, central Turkey and Neogene tectonics of the Anatolian collage. J. Volcanol. Geotherm. Res. 117, 237–262.

Piper, J.D.A., Koçbulut, F., Gürsoy, H., Tatar, O., Viereck, L., Lepetit, P., Roberts, A.P., Akp\inar, Z., 2013. Palaeomagnetism of the Cappadocian Volcanic Succession, Central Turkey: Major ignimbrite emplacement during two short (Miocene) episodes and Neogene tectonics of the Anatolian collage. J. Volcanol. Geotherm. Res. 262, 47–67.

Platzman, E.S., Tapirdamaz, C., Sanver, M., 1998. Neogene anticlockwise rotation of central Anatolia (Turkey): preliminary palaeomagnetic and geochronological results. Tectonophysics 299, 175–189.

Poisson, A., Guezou, J.C., Ozturk, A., Inan, S., Temiz, H., Gürsöy, H., Kavak, K.S., Özden, S., 1996. Tectonic Setting and Evolution of the Sivas Basin, Central Anatolia, Turkey. Int. Geol. Rev. 38, 838–853. https://doi.org/10.1080/00206819709465366

Poisson, A., Vrielynck, B., Wernli, R., Negri, A., Bassetti, M.-A., Büyükmeriç, Y., Özer, S., Guillou, H., Kavak, K.S., Temiz, H., Orszag-Sperber, F., 2016. Miocene transgression in the central and eastern parts of the Sivas Basin (Central Anatolia, Turkey) and the Cenozoic palaeogeographical evolution. Int. J. Earth Sci. 105, 339–368. https://doi.org/10.1007/s00531-015-1248-1

Pourteau, A., Sudo, M., Candan, O., Lanari, P., Vidal, O., Oberhänsli, R., 2013. Neotethys closure history of Anatolia: insights from 40 Ar- 39 Ar geochronology and P-T estimation in high-pressure metasedimentary rocks. J. Metamorph. Geol. 31, 585–606. https://doi.org/10.1111/jmg.12034

Ribes, C., Kergaravat, C., Bonnel, C., Crumeyrolle, P., Callot, J.-P., Poisson, A., Temiz, H., Ringenbach, J.-C., 2015. Fluvial sedimentation in a salt-controlled mini-basin: stratal patterns and facies assemblages, Sivas Basin, Turkey. Sedimentology 62, 1513–1545.

Robertson, A.H.F., 2002. Overview of the genesis and emplacement of Mesozoic ophiolites in the Eastern Mediterranean Tethyan region. Lithos 65, 1–67. https://doi.org/10.1016/S0024-4937(02)00160-3

Robertson, A.H.F., Parlak, O., Ustaomer, T., 2009. Melange genesis and ophiolite emplacement related to subduction of the northern margin of the Tauride-Anatolide continent, central and western Turkey. Geol. Soc. London, Spec. Publ. 311, 1. https://doi.org/10.1144/SP311.Erratum

Sarıkaya, M.A., Yıldırım, C., Çiner, A., 2015. No surface breaking on the Ecemiş Fault, central Turkey, since Late Pleistocene (~ 64.5 ka); new geomorphic and geochronologic data from cosmogenic dating of offset alluvial fans. Tectonophysics 649, 33–46.

Schildgen, T.F., Cosentino, D., Caruso, a., Buchwaldt, R., Yıldırım, C., Bowring, S. a., Rojay, B., Echtler, H., Strecker, M.R., 2012. Surface expression of eastern Mediterranean slab dynamics: Neogene topographic and structural evolution of the southwest margin of the Central Anatolian Plateau, Turkey. Tectonics 31, TC2005.

https://doi.org/10.1029/2011TC003021

Şengör, A.M.C., Yılmaz, Y., 1981. Tethyan evolution of Turkey: a plate tectonic approach. Tectonophysics 75, 181–241.

Tauxe, L., 2010. Essentials of paleomagnetism. Univ of California Press.

Tauxe, L., Watson, G.S., 1994. The fold test: an eigen analysis approach. Earth Planet. Sci. Lett. 122, 331–341.

5   Topuz, G., Okay, A.I., Altherr, R., Schwarz, W.H., Sunal, G., Altinkaynak, L., Altınkaynak, L., 2014. Triassic warm subduction in northeast Turkey: Evidence from the Ağvanis metamorphic rocks. Isl. Arc 23, n/a--n/a. https://doi.org/10.1111/iar.12068

Torsvik, T.H., der Voo, R., Preeden, U., Mac Niocaill, C., Steinberger, B., Doubrovine, P. V, van Hinsbergen, D.J.J., Domeier, M., Gaina, C., Tohver, E., others, 2012. Phanerozoic polar wander, palaeogeography and dynamics. Earth-Science

10   Rev. 114, 325–368.

Ustaömer, T., Robertson, A.H.F., 2010. Late Palaeozoic-Early Cenozoic tectonic development of the Eastern Pontides (Artvin area), Turkey: stages of closure of Tethys along the southern margin of Eurasia. Geol. Soc. London, Spec. Publ. 340, 281–327.

Ustaömer, T., Robertson, A.H.F., 1997. Tectonic-Sedimentary Evolution of the North Tethyan Margin in the Central

15   Pontides of Northern Turkey. AAPG Mem. 68, 255–290.

van der Voo, R., 1968. Paleomagnetism and the Alpine tectonics of Eurasia IV: Jurassic, Cretaceous and Eocene pole positions from northeastern Turkey. Tectonophysics 6, 251–269.

Van der Voo, R., 1990. The reliability of paleomagnetic data. Tectonophysics 184, 1–9.

van Hinsbergen, D.J.J., Maffione, M., Plunder, A., Kaymakci, N., Ganerød, M., Hendriks, B.W.H., Corfu, F., Gürer, D., Gelder,

20   G.I.N.O. de, Peters, K., Others, Hinsbergen, D.J.J. van, Maffione, M., Plunder, A., Kaymakci, N., Ganerød, M., Hendriks, B.W.H., Corfu, F., Gürer, D., Gelder, G.I.N.O. de, Peters, K., Others, Kaymakcı, N., Ganerød, M., Hendriks, B.W.H., Corfu, F., Gürer, D., Gelder, G.I.N.O. de, Peters, K., McPhee, P.J., Brouwer, F.M., Advokaat, E.L., Vissers, R.L.M., 2016. Tectonic evolution and paleogeography of the Kırşehir Block and the Central Anatolian Ophiolites, Turkey. Tectonics 35, 983–1014. https://doi.org/10.1002/2015tc004018

25   Van Velzen, A.J., Zijderveld, J.D.A., 1995. Effects of weathering on single-domain magnetite in Early Pliocene marine marls. Geophys. J. Int. 121, 267–278.

Whitney, D.L., Hamilton, M.A., 2004. Timing of high-grade metamorphism in central Turkey and the assembly of Anatolia. J. Geol. Soc. London 161, 823–828.

Yilmaz, A., Yilmaz, H., 2006. Characteristic features and structural evolution of a post collisional basin: The Sivas Basin,

30   Central Anatolia, Turkey. J. Asian Earth Sci. 27, 164–176.

Zijderveld, J.D.A., 1967. AC demagnetization of rocks: analysis of results, in: Collinson, D.W., Creer, K.M. (Eds.), Methods in Paleomagnetism. Elsevier, Amsterdam, pp. 254–286.
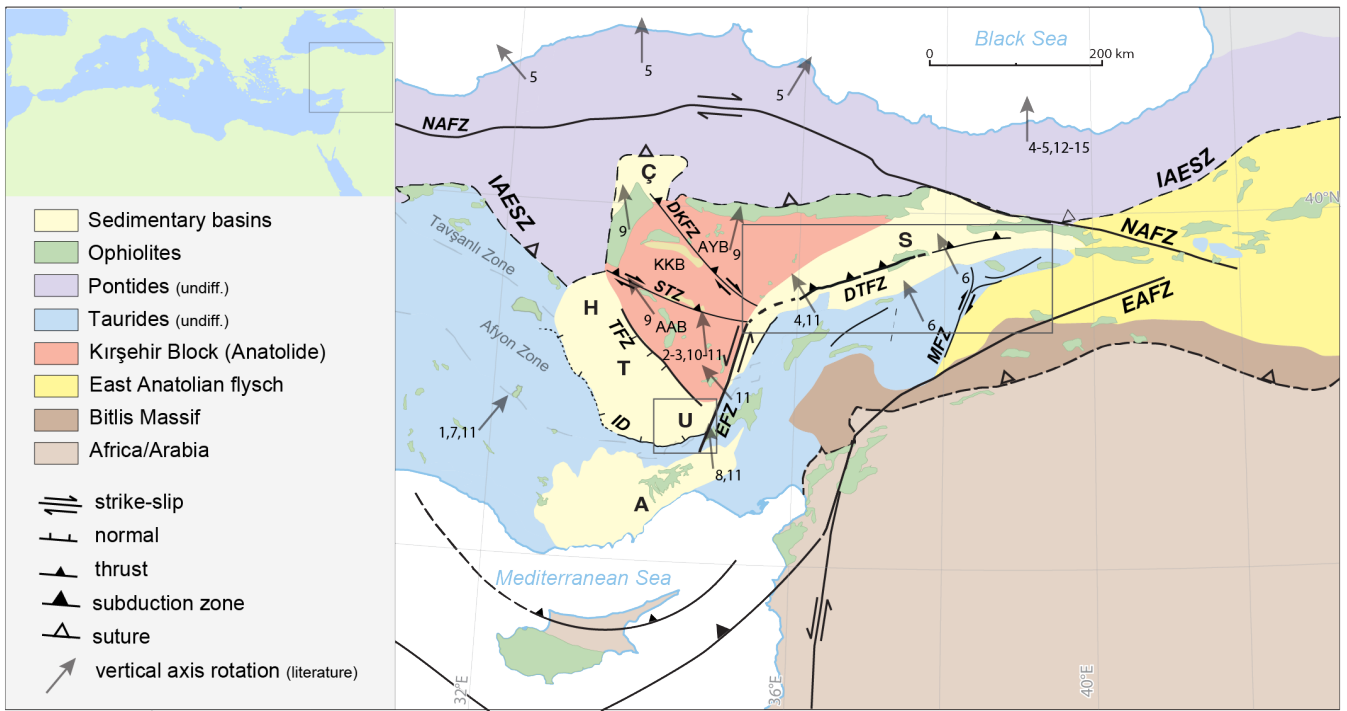
Figure 1: Tectonic units, associated suture zones, main fault zones within the Anatolian microplate. Available vertical axis rotations are shown as arrows, corresponding references are: (**1:** Kissel et al., 1993; **2:** Platzman et al., 1998; **3:** Piper et al., 2002; **4:** Kissel et al., 2003; **5:** Meijers et al., 2010a; **6:** Gürsoy et al., 2011; **7:** Meijers et al., 2011; **8:** Lucifora et al., 2012; **9:** Lefebvre et al., 2013; **10:** Piper et al., 2013; **11:** Çinku et al., 2016 **12:** Baydemir, 1990; **13:** Channell et al., 1996; **14:** Orbay and Bayburdi, 1979; **15:** van der Voo, 1968). Locations of the sedimentary basins mentioned: Ulukışla (U), Sivas (S), Haymana (H), Tuzgölü (T), Çankırı (Ç), Adana (A). Major faults: Ecemiş Fault Zone (EFZ), Deliler-Tecer Fault Zone (DTFZ), Savcılı Thrust Zone (STZ), Tuzgölü Fault (TFZ), North Anatolian Fault Zone (NAFZ), East Anatolian Fault Zone (EAFZ), Malatya Fault Zone (MFZ), Ivriz Detachment (ID). The Kırşehir Block consists from north to south of the Akadağ-Yozgat Block (AYB), the Kırşehir–Kırıkkale Block (KKB), and the Ağaçören–Avanos Block (AAB). Note that the U and S basins are offset along the EFZ. Map insets of the geology of the study regions between the Kırşehir Block and the Taurides, and the Kırşehir Block, the Eastern Pontides and Taurides are shown in **Figs. 2 and 3.**
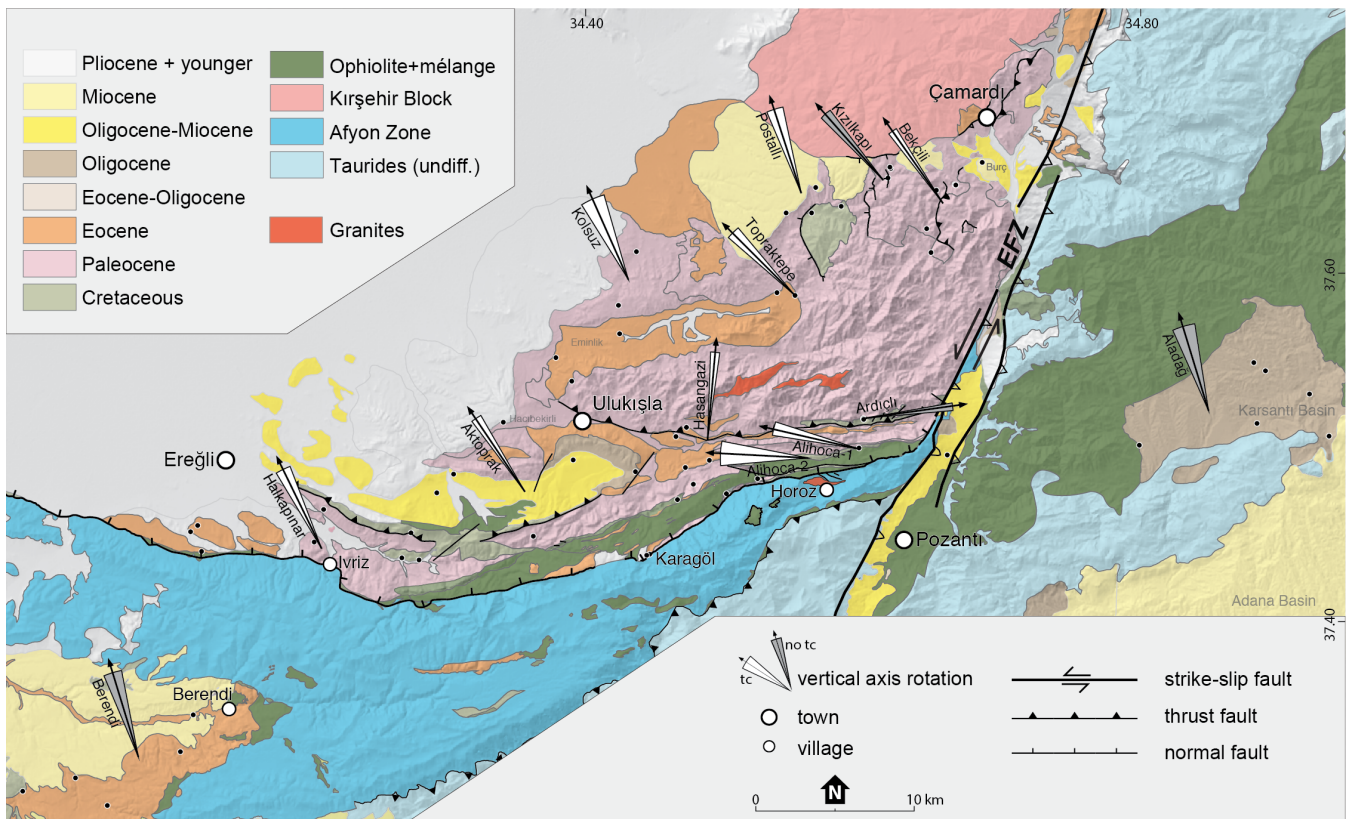
Figure 2: Geological map of the Ulukışla Basin (modified after Gürer et al., 2016) with major tectonic structures. Individual sampling sites are shown as black dots, localities and associated vertical axis rotations are denoted as arrows with their 95% error envelope (DD$_x$).
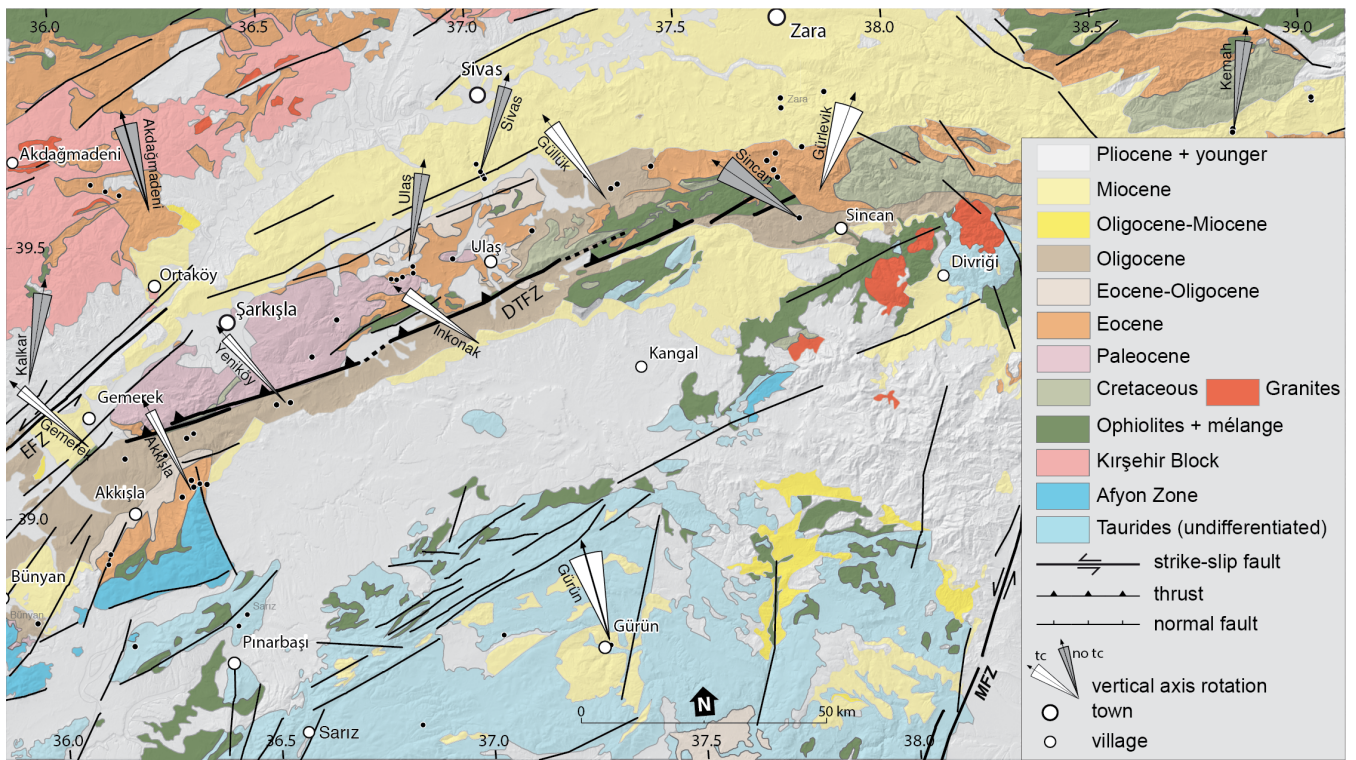
Figure 3: Geological map of the Sivas Basin with major tectonic structures (modified from MTA, 2002). Symbols are as in caption to **Fig 2.**
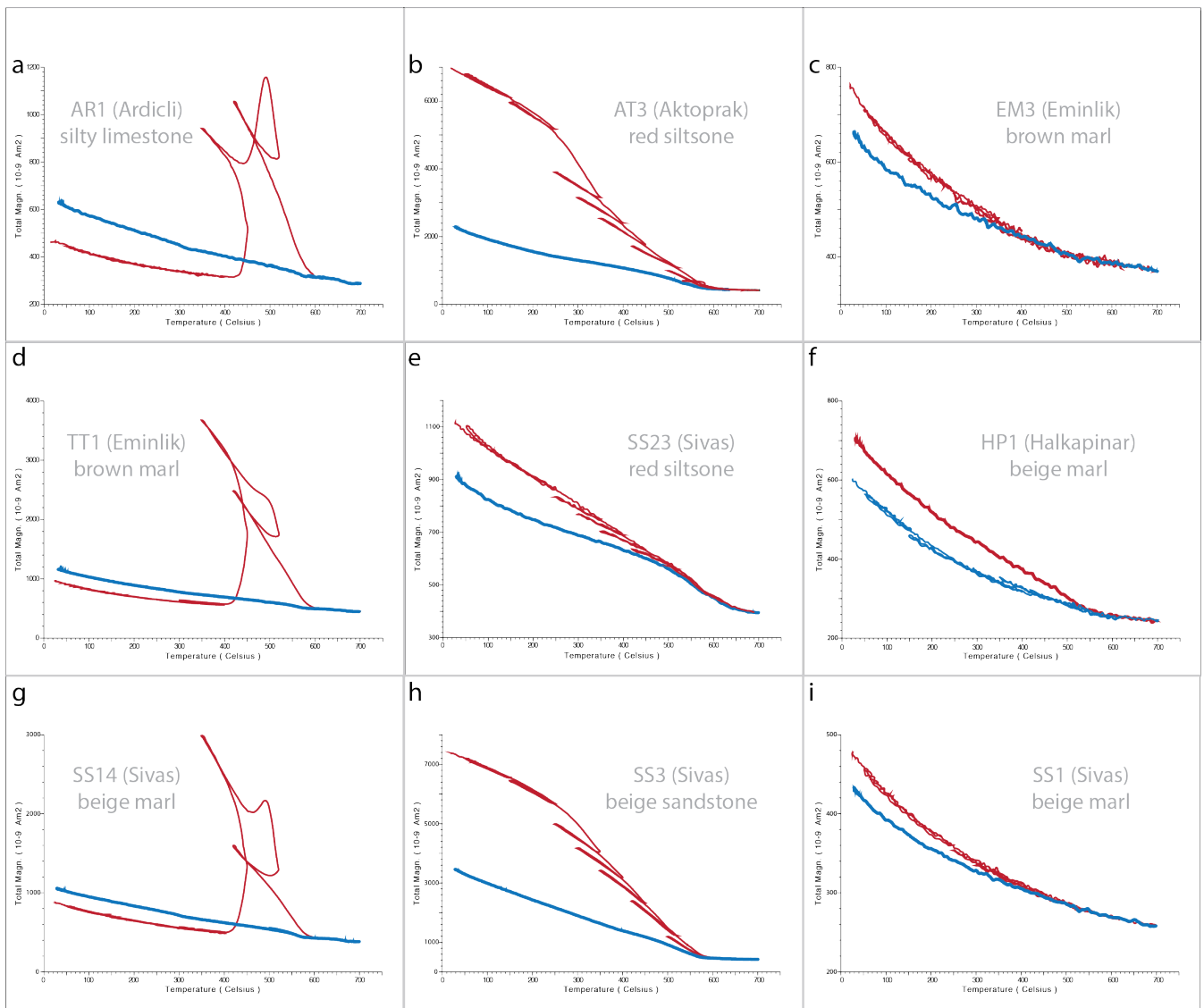
Figure 4: Magnetic carriers identified by their characteristic thermomagnetic curves generated with the stepwise heating protocol (Mullender et al., 1993) for representative samples. Heating is represented by red line. The final cooling segment is indicated by the blue line. A noisy appearance is indicative of a weak magnetic signal. See for text for explanation of the thermomagnetic behaviour.
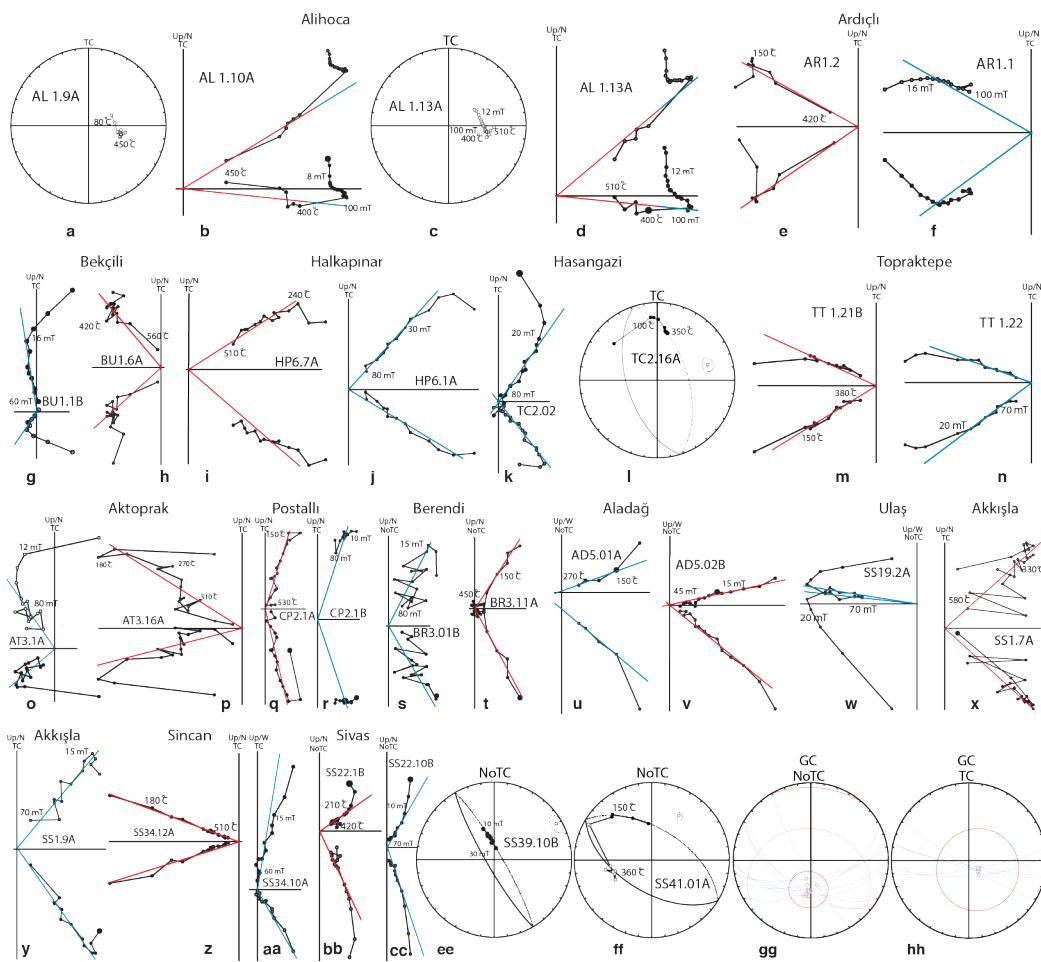
Figure 5: Zijderveld diagrams (Zijderveld, 1967) of representative samples demagnetized using thermal (red lines, TH) and alternating field (blue lines, AF) demagnetization shown in in situ (noTC) or tectonic (TC) coordinates. The solid and open dots represent projections on the horizontal and vertical planes, respectively. Great circle plots of g, h, and jj, use the technique of McFadden and McElhinny (1988). Demagnetization step values are in °C or in mT. See text for further explanation.

Figure 6: Locality results from sedimentary basins (Ulukışla and Sivas basins, and basins overlying the Tauride fold-and-thrust belt). Equal area projections of ChRM directions and their means with associated error ellipses (DD_x, DI_x) according to (Deenen et al., 2011), either before (orange; NoTC) or after tectonic correction (blue; TC). Rejected directions (after 45° cut-off) are displayed in grey, positive (negative) inclinations are shown as solid (open) circles. All directions have been converted to normal polarity (see also **Table 1**).
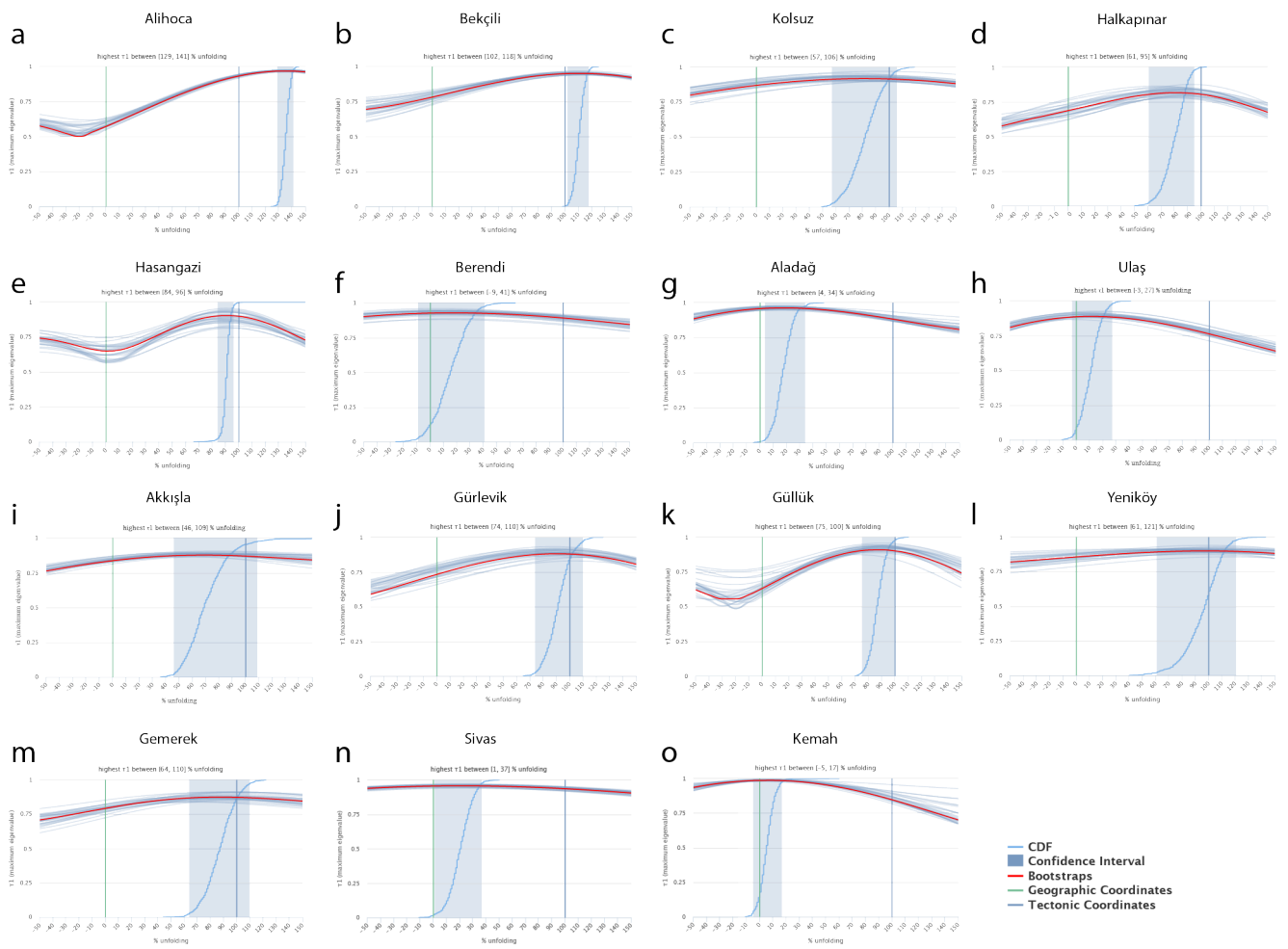
Figure 7: Representative fold-tests after Tauxe et al. (2010) for localities from the Ulukışla and Sivas basins.
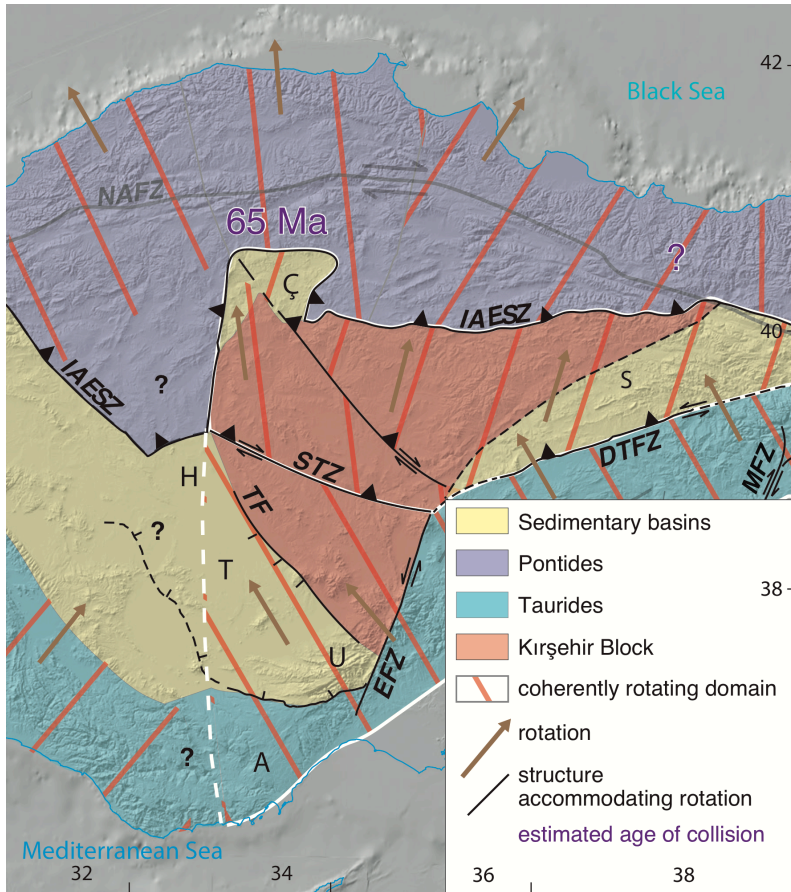
Figure 8: Coherently rotating domains within the Anatolian orogen and tectonic structures accommodating differential rotations. NAFZ - North Anatolian Fault Zone, IAESZ – Izmir-Ankara-Erzincan Suture Zone, STZ – Savcılı Thrust Zone, DTFZ – Deliler-Tecer Fault Zone, TF – Tuzgölü Fault, EFZ – Ecemiş Fault zone, Malatya Fault Zone (MFZ). Basins: U – Ulukışla, T - Tuzgölü, H - Haymana, A - Adana. Orange hatching indicates the amount of vertical axis rotation of each domain, whereby the hatching is rotated from N-S according to the paleomagnetic results summarized in **Table 1**.
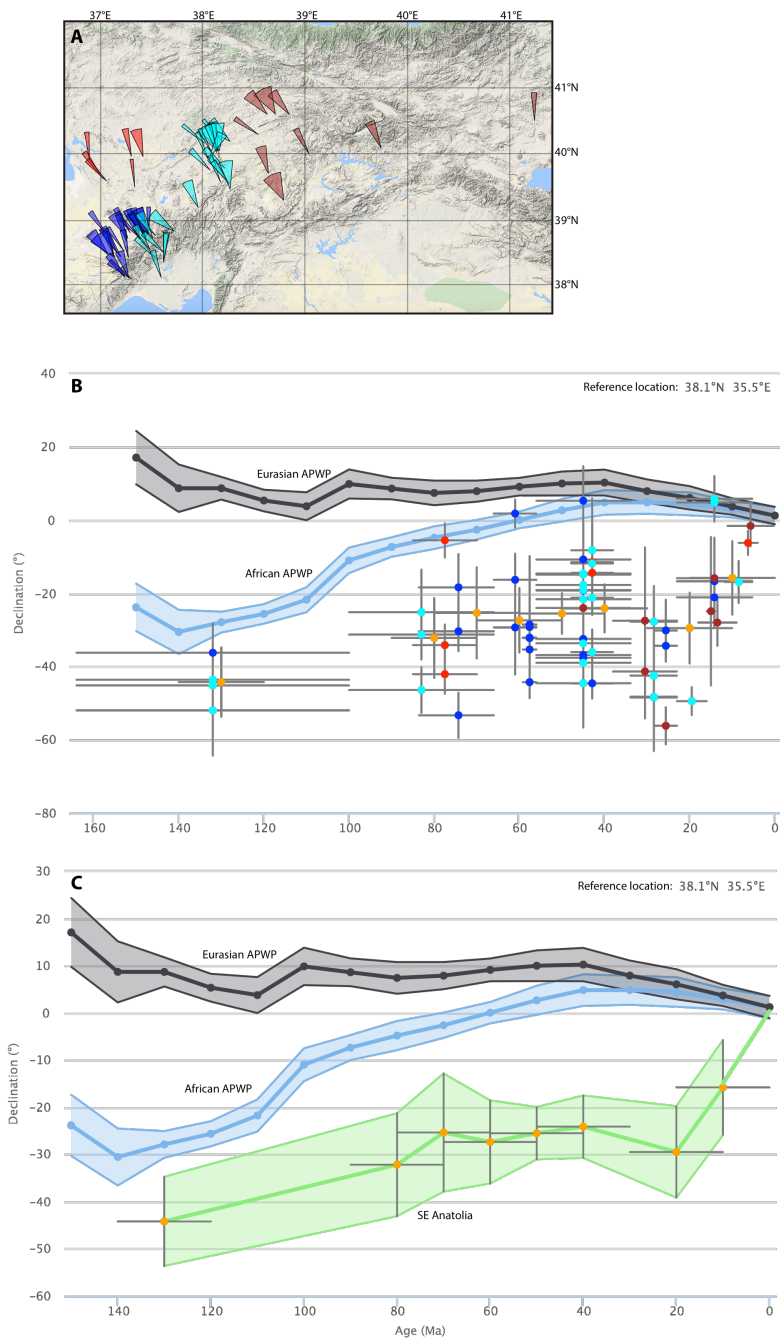
Figure 9: a) Published and new paleomagnetic sites from the SE Anatolian rotating domain used to calculate an Apparent Polar Wander Path for the block of Fig. c). Color coding subdivides the sites in four regions. This allows showing in Fig. b) that there the APWP is not significant biased by deviating declinations of one region. Reference APWPs for Africa and Eurasia come from Torsvik et al. (2012).

Site	Age	lat (°)	long (°)	Na	Ni	N45	D	ΔDx	I	ΔIx	D	ΔDx	I	ΔIx	K	A95	A95min	A95max	Rot	ΔRot	sense
							geographic coordinates				tectonic coordinates										
ULUKISLA BASIN																					
Alihoca-1	**Coniacian-Maastrichtian**	37.5	34.7	111	47	47					283.1	4.4	40.3	5.6	27.4	4.0	2.6	7.3	86.9	4.4	ccw
AL1		37.505	34.733	24	24	24	19.4	3.7	-23.8	6.3	91.5	4.8	-47.4	5.0	50.5	4.2	3.4	11.1			
AL3		37.485	34.697	46			no result															
AL4 (recent)		37.471	34.659	16			355.6	9.0	60.9	5.7											
AR2		37.513	34.822	25	23	23	217.7	4.5	42.6	5.4	292.8	3.7	31.9	5.5	75.5	3.5	3.4	11.4			
Alihoca-2	**Selandian (L. Paleocene)**	37.5	34.7	19	15	13					265.7	5.2	46.4	5.6	81.1	4.6	4.3	16.3	84.3	5.2	ccw
AL2		37.506	34.734	19	15	13	19.7	7.2	-18.4	13.1	85.7	5.2	-46.4	5.6	81.1	4.6	4.3	16.3			
Ardıçlı	**Campanian-Maastrichtian**	37.6	34.8	34	22	22	82.6	2.5	47.7	2.6					195.8	2.2	3.5	11.7	82.6	2.5	cw
AR1		37.541	34.828	19	14	14	261.8	3.0	-48.0	3.1	222.0	2.7	-31.6	4.1	233.8	2.6	4.2	15.6			
AR3		37.540	34.828	15	8	8	264.1	5.2	-47.3	5.4	230.7	4.7	-28.2	7.6	149.6	4.5	5.2	22.1			
Bekcili	**Thanetian (L. Paleocene)**	37.8	34.9	139	70	70					324.6	2.9	37.7	3.9	39.9	2.7	2.2	5.6	35.4	2.9	ccw
BU1		37.767	34.945	23	5	5	297.8	13.3	36.3	18.4	329.8	19.3	41.5	23.6	19.9	17.6	6.3	29.7			
BU2		37.766	34.946	33	6	6	147.4	13.7	0.1	27.4	154.1	14.6	-25.8	24.4	23.2	14.2	5.9	26.5			
YK1		37.701	34.914	14	13	13	162.6	4.1	-16.3	7.6	147.8	5.1	-36.5	7.1	75.4	4.8	4.3	16.3			
YK2		37.724	34.910	13	13	13	164.6	5.1	-19.5	9.2	147.6	6.6	-40.0	8.4	47.0	6.1	4.3	16.3			
YK3		37.761	34.922	29	20	20	13.9	5.2	57.6	3.8	315.8	3.6	44.7	4.0	105.3	3.2	3.6	12.4			
YK4		37.766	34.146	27	13	13	309.4	5.3	14.0	10.1	324.3	5.5	28.7	8.7	62.7	5.3	4.3	16.3			
Kızılkapı	**Thanetian (L. Paleocene)**	37.8	34.8	115	55	54	314.5	5.4	46.5	5.7					16.3	5.0	2.5	6.7	45.5	5.4	ccw
CP1		37.785	34.866	16	12	12	130.2	10.0	-36.8	13.6	172.7	19.4	-61.2	12.0	10.3	14.2	4.4	17.1			
PC1		37.742	34.769	31	26	23	52.5	9.5	-46.7	10.1	357.1	15.3	-64.8	8.0	9.5	10.4	3.4	11.4			
PC2		37.774	34.809	22	19	19	114.9	5.6	-49.6	5.4	172.8	11.8	-68.8	5.0	22.8	7.2	3.7	12.8			
PC3		37.774	34.864	20			no result															
PC4		37.783	34.867	26	24	24	154.1	5.2	-46.0	5.7	209.5	7.4	-60.7	4.7	29.9	5.5	3.4	11.1			
Kolsuz	**Paleocene**	37.7	34.5	48	18	18					335.8	7.8	32.5	11.7	22.4	7.5	3.8	13.3	24.2	7.8	ccw
KL1		37.655	34.531	28	8	8	157.6	6.6	-23.8	11.2	163.6	7.1	-36.0	9.9	70.1	6.7	5.2	22.1			
EM3		37.707	34.554	20	10	10	132.3	15.1	-45.7	16.5	149.7	1.5	-29.2	20.2	16.4	12.3	4.8	19.2			
Halkapınar	**Eocene**	37.4	34.3	196	69	68					334.8	4.9	33.4	7.3	14.4	4.7	2.2	5.7	25.2	4.9	ccw
YL1 (remagnetized)		37.422	34.019	11	5	5	175.5	7.2	-53.1	6.2	176.7	4.5	-25.1	7.5	312.6	4.3	6.3	29.7			
HP1		37.437	34.274	31	24	24	158.0	8.9	44.6	10.1	160.9	6.9	-36.6	9.4	22.1	6.4	3.4	11.1			
HP2		37.411	34.283	21	6	6	305.5	49.5	73.2	14.5	330.4	15.6	31.5	23.7	21.1	14.9	5.9	26.5			
HP3		37.461	34.168	26	16	15	168.8	8.6	-3.8	17.0	142.0	12.0	-50.5	11.4	14.8	10.3	4.1	14.9			
HP4 (remagnetized)		37.430	34.156	14	14	7	156.1	2.8	-65.4	1.4	182.3	1.3	9.2	2.5	2180.3	1.3	5.5	24.1			
HP5		37.413	34.262	13	13		no result															
HP6		37.432	34.423	20	11	11	147.7	8.5	-0.8	16.9	153.2	10.5	-38.8	13.7	23.1	9.7	4.6	18.1			
KG1 (recent)		37.413	34.564	30	20	20	0.3	4.9	56.6	3.7	341.2	2.2	16.4	4.1	71.9	3.9	3.6	12.4			
KG2		37.412	34.561	30	12	12	182.6	15.5	-70.1	6.1	168.9	6.4	-35.4	9.0	53.4	6.0	4.4	17.1			
Eminlik	**Eocene**	37.6	34.6	70																	
EM1 (recent)		37.665	34.725	17			355.2	5.1	52.6	4.5											
EM2 (remagnetized)		37.628	34.532	16	8	8	179.4	12.5	-56.1	9.6	162.5	8.2	-7.5	16.2	-72.3	8.2	5.2	22.1			
EM4 (remagnetized)		37.606	34.454	23	23	23	191.7	11.7	-67.4	5.4	179.2	3.7	-14.7	7.0	68.0	3.7	3.4	11.4			
EM5 (recent)		37.582	34.473	14			352.3	9.1	60.4	5.9											
Hasangazi	**Eocene**	37.5	34.6	110	41	38					4.9	2.8	31.4	4.2	77.8	2.6	2.8	8.3	4.9	2.8	cw
HG1 (recent)		37.536	34.612	10	9	9	356.3	4.7	60.6	3.0	90.3	45.8	85.8	3.0	75.9	5.9	5.0	20.5			
HG2		37.527	34.599	16	16	13	183.2	4.4	21.4	7.8	185.1	5.1	-37.7	6.9	75.9	4.8	4.3	16.3			
TC1		37.497	34.610	22	22		no result															
TC2		37.503	34.639	27	25	25	240.6	4.9	-58.6	3.4	184.8	3.2	-28.2	5.2	87.9	3.1	3.3	10.8			
GM1		37.466	34.599	16			no result															
GM2 (recent)		37.480	34.619	19	7	7	2.7	11.9	57	8.9	352.2	4.1	2	8.1	222.8	4.1	5.5	24.1			
Topraktepe	**Middle Eocene**	37.7	34.8	30	29	28					315.5	4.1	42.8	4.9	53.4	3.8	3.2	10.0	44.5	4.1	ccw
TT1		37.660	34.750	30	29	28	4.6	3.3	26.7	5.4	315.5	4.1	42.8	4.9	53.4	3.8	3.2	10.0			
Aktoprak	**Chattian (L. Oligocene)**	37.5	34.4	398	148	144					326.3	3.8	46.6	4.0	13.5	3.3	1.6	3.6	33.7	3.8	ccw
AT1		37.493	34.549	15			no result															
AT2		37.506	34.473	22			no result															
AT3		37.494	34.327	27	27	26	48.1	12.1	-60.1	7.9	150.3	8.3	-34.6	11.9	14.0	7.9	3.3	10.5			
AT4 (recent)		37.476	34.306	21	20	20	4.9	3.0	57.0	3.1	10.0	1.5	2.4	3.1	454.9	1.5	3.6	12.4			
Kurtulmus Tepe (Meijers et al., 2016)		37.522	34.475	313	129	121	338	2.7	18.5	5.0	326.4	4.3	49.6	4.2	12.8	3.7	1.8	4.0			
Postallı	**Miocene**	37.8	34.8	40	27	27					342.3	5.8	36	8.1	27.2	5.4	3.2	10.3	17.7	5.4	ccw
CP2		37.757	34.772	16	12	12	144.3	21.1	-68.6	9.0	163.6	10.2	-43.3	12.0	23.0	9.2	4.4	17.1			
CP3		37.742	34.738	24	15	15	359.5	9.6	51.8	8.8	341.5	6.7	30.2	10.5	35.8	6.5	4.1	14.9			
Burç	**Miocene**																				
BU3		37.788	34.979	17			no result															
Hacıbekirli	**Miocene**	37.5	34.4	24	18	18	2.8	4.1	52.6	3.6									2.8	4.1	cw
HB1		37.544	34.388	24	18	18	182.8	4.1	-52.6	3.6	164.8	3.1	-34.1	4.5	137.2	3.0	3.8	13.3			
Ulukisla_all_directions	**Paleocene-Oligocene**	37.6	34.7	334	326						327.7	2.2	40.5	2.7	16.4	2.0	1.2	2.1	32.3	2.2	ccw
Ulukisla_all_sites	**Paleocene-Oligocene**	37.6	34.7	16	16						330.4	4.8	38.0	6.4	4.6 (α95)	66 (k)			29.6	4.8	ccw
Ulukisla_all_localities	**Paleocene-Oligocene**	37.6	34.7	5	5						327.8	9.0	38.8	11.8	84.4 (α95)	8.4 (k)			32.2	9.0	ccw

Site	Age	lat (°)	long (°)	Na	Ni	N45	D	ΔDx	I	ΔIx	D	ΔDx	I	ΔIx	K	A95	A95min	A95max	Rot	ΔRot	sense
							geographic coordinates				tectonic coordinates										
TAURIDE FTB and OVERLYING BASINS																					
Berendi	**Thanetian (L. Paleocene)-Ypresian (E.Eocene)**	37.2	33.9	58	40	39	343.1	6.2	53.7	5.3					21.0	5.1	2.8	8.2	16.9	6.2	ccw
BR1		37.266	34.047	12	6	6	161.0	16.1	-43.0	19.0	136.0	11.6	-34.0	16.8	38.4	10.9	5.9	26.5			
BR2		37.262	34.006	10	6	6	176.6	8.8	-65.5	4.5	163.5	6.0	-51.9	5.4	174.6	5.1	5.9	26.5			
BR3		37.227	33.990	14	10	10	157.6	6.3	-57.6	4.6	160.0	4.2	-41.7	5.1	159.9	3.8	4.8	19.2			
BR4		37.202	33.862	13	12	12	163.0	6.4	-52.6	5.6	184.0	5.8	-43.3	6.8	68.9	5.3	4.4	17.1			
BR5 (recent)		37.175	33.900	9	9	9	0.0	4.3	52.9	3.8	354.8	3.6	45.2	4.0	256.2	3.2	5.0	20.5			
BR6		37.190	33.798				no result															
Aladağ	**Oligocene**	37.5	35.3	56	20	20	343.4	7.3	52.9	6.3					29.9	6.1	3.6	12.4	16.6	7.3	ccw
AD1		37.587	35.305	16			no result															
AD3 (norm)		37.513	35.395	18			no result															
AD4		37.555	35.372	13	13	13	341.6	10.5	57.0	7.8	351.6	5.3	28.7	8.4	67.9	5.1	4.3	16.3			
AD5		37.527	35.307	9	7	7	345.9	7.4	45.5	8.1	309.2	5.8	34.7	8.3	121.7	5.5	5.5	24.1			
Sarız	**L.Cretaceous-Eocene**	38.7	36.7	63																		
SS06		38.592	36.834	21			no result															
SS07		38.809	36.430	17			no result															
SS08		38.788	36.409	16			no result															
SS09		38.752	37.035	9			no result															
Gürün	**Miocene**	38.7	37.3	11	9	9					343.9	10.9	42.9	12.9	32.2	9.9	5.2	22.1	16.1	10.9	ccw
SS10		38.724	37.286	11	8	8	146.9	12.0	-53.1	10.3	163.9	10.9	-42.9	12.9	32.2	9.9	5.2	22.1			
SIVAS BASIN																					
Ulaş	**Paleocene-Eocene**	39.4	36.8	207	45	43	8.8	5.3	40.1	6.7					21.1	4.9	2.7	7.7	8.8	5.3	cw
SS11		39.466	37.006	20			no result															
SS17		39.440	36.856	32	12	12	187.9	14.5	-62.3	8.6	222.2	6.5	-28.2	10.5	48.3	6.3	4.4	17.1			
SS18		39.428	36.856	31			no result															
SS19		39.421	36.830	21	15	15	190.9	6.7	-33.2	9.9	174.5	6.2	-32.1	9.3	42.8	5.9	4.1	14.9			
SS20		39.417	36.816	25	13	13	186.7	8.6	-31.9	13	184.5	7.6	13.5	14.5	30.9	7.6	4.3	16.3			
SS21		39.419	36.803	27			no result															
SS29		39.347	36.669	17	5	5	179.7	12	-26.1	19.9	207.9	15	-31.7	22.7	29.5	14.3	6.3	29.7			
SS30		39.280	36.607	17			no result															
SS31 (recent)		39.451	36.952	17	17	17	3.6	5.9	52.4	5.3	355.6	13.4	74.5	3.9	31.7	6.4	3.9	13.8			

Site	Age	lat (°)	long (°)	Na	Ni	N45	D	ΔDx	I	ΔIx	D	ΔDx	I	ΔIx	K	A95	A95min	A95max	Rot	ΔRot	sense
SIVAS BASIN (cont.)																					
Akkışla	**Eocene**	**39.0**	**36.2**	**126**	**95**	**89**					**333.6**	**3.4**	**30.1**	**5.3**	**21.9**	**3.3**	**2.0**	**4.8**	**26.4**	**3.4**	**ccw**
SS1		39.054	36.329	21	15	15	210.3	13.5	-64.8	7.1	165.0	6.7	-38.4	8.9	38.3	6.3	4.1	14.9			
SS4 (recent)		*38.910*	*36.106*	*10*	*6*	*6*	*1.6*	*14.9*	*55.2*	*11.9*	*27.2*	*13.9*	*51.6*	*12.7*	*33.5*	*11.7*	*5.9*	*26.5*			
SS5		38.929	36.112	21	19	19	347.5	6.6	51.2	6.1	338.5	4.5	32.3	6.8	61.7	4.3	3.7	12.8			
SS25		38.757	36.162	20	18	18	146.7	6.8	-17.5	12.6	137.2	6.7	-13.2	12.8	28.1	6.6	3.8	13.3			
SS27		39.061	36.309	17	17	17	0.8	3.7	55.0	3.0	341.1	2.3	36.5	3.2	265.0	2.2	3.9	13.8			
SS55		39.049	36.314	12	8	8	332.6	19.7	49.1	19.4	326.5	14.8	29.4	23.3	16.2	14.2	5.2	22.1			
SS56		39.031	36.286	14	8		355.0	10.4	44	12	342.0	7.1	23.0	12.3	35.9	9.4	5.2	22.1			
SS57		39.053	36.346	11	10	10	336.0	12.1	33.9	17.6	342.1	27.6	65.6	13.7	8.1	18.1	4.8	19.2			
Gürlevik	**Eocene**	**39.6**	**37.7**	**76**	**20**	**19**					**199.8**	**9.5**	**-40.2**	**12.1**	**15.6**	**8.8**	**3.7**	**12.8**	**19.8**	**9.5**	**cw**
SS33		39.605	37.712	18	12	11	217.0	17.0	-44.3	19.4	186.2	15.4	-38.4	20.2	11.2	14.2	4.6	18.1			
SS36		*39.627*	*37.798*	*18*			*no result*														
SS43		*39.617*	*37.733*	*18*			*no result*														
SS44		39.587	37.727	12	8	8	205.7	5.2	6.4	10.4	207.2	7.7	-41.4	9.5	62.2	7.1	5.2	22.1			
SS45		*39.559*	*37.727*	*10*			*no result*														
Güllük	**L.Eo-Oligocene**	**39.6**	**37.3**	**69**	**24**	**24**					**322.4**	**10.7**	**53.9**	**9.0**	**12.2**	**8.8**	**3.4**	**11.1**	**37.6**	**10.7**	**ccw**
SS32		*39.496*	*37.144*	*18*	*18*	*17*	*244.9*	*7.9*	*-63.2*	*4.5*	*275.1*	*4.5*	*-10.0*	*8.8*	*59.4*	*4.5*	*3.8*	*13.3*			
SS51		39.593	37.278	14	14	12	251.9	16.8	-65.4	8.6	137.3	12.7	-49.9	12.3	14.2	10.9	4.2	15.6			
SS52		*39.567*	*37.336*	*13*	*13*	*13*	*230.2*	*6.3*	*0.0*	*12.6*	*224.9*	*4.5*	*-13.9*	*8.6*	*86.1*	*4.5*	*4.3*	*16.3*			
SS53		*39.575*	*37.352*	*11*	*11*	*11*	*172.1*	*10.7*	*-39.6*	*13.8*	*99.6*	*13.3*	*-43.7*	*15.4*	*15.4*	*12.0*	*4.6*	*18.1*			
SS54		39.605	37.434	13	10	10	328.6	8.5	8.7	16.6	331.5	19.6	59.0	13.4	11.4	14.9	4.8	19.2			
Akdağmadeni	**Eocene**	**39.6**	**36.1**	**74**	**33**	**33**	**345.2**	**7.2**	**54.1**	**6.0**					**20.3**	**5.7**	**3.0**	**9.1**	*14.8*	*7.2*	*ccw*
SS14		39.613	36.093	31	22	22	160.7	9.6	-51.7	8.7	163.7	6.8	-22.1	11.9	22.7	6.7	3.5	11.7			
SS15		39.600	36.128	21	11	11	175.0	8.1	-58.0	5.8	185.4	5.6	-34.8	7.9	76.4	5.3	4.6	18.1			
SS16		*39.592*	*36.161*	*22*			*no result*														
Sincan	**Oligocene**	**39.5**	**37.8**	**16**	**16**	**16**	**304.2**	**9.0**	**47.8**	**9.3**					**22.6**	**6.4**	**4.0**	**14.3**	*55.8*	*9.0*	*ccw*
SS34		39.496	37.783	16	16	16	304.2	9.0	47.8	9.3	277.5	6.6	25.7	11.0	22.6	6.4	4.0	14.3			
Yeniköy	**Oligocene**	**39.2**	**36.4**	**189**	**93**	**89**					**317.6**	**3.5**	**41.1**	**4.4**	**22.5**	**3.2**	**2.0**	**4.8**	**42.4**	**3.2**	**ccw**
SS02		*39.109*	*36.249*	*28*	*28*	*28*	*12.2*	*1.7*	*53.3*	*1.4*	*14.9*	*1.1*	*37.5*	*1.5*	*681.4*	*1.0*	*3.2*	*10.0*			
SS03 (recent)		*39.147*	*36.318*	*22*	*18*	*18*	*355.6*	*3.6*	*53.7*	*3.1*	*347.3*	*1.9*	*12.2*	*3.7*	*321.5*	*1.9*	*3.8*	*13.3*			
SS26 (recent)		*39.105*	*36.153*	*21*	*21*	*21*	*10.1*	*2.9*	*54.6*	*2.4*	*2.3*	*3.3*	*57.5*	*2.4*	*148.6*	*2.6*	*3.6*	*12.0*			
SS28 (recent)		*39.139*	*36.301*	*5*	*5*	*5*	*0.3*	*11.9*	*53.0*	*8.3*	*350.7*	*21.9*	*24.1*	*37.3*	*13.8*	*21.3*	*6.3*	*29.7*			
SS58		39.198	36.551	5	5	5	314.5	11.0	-9.5	21.5	311.6	14.5	35.1	20.6	32.3	13.7	6.3	29.7			
SS59 (recent)		*39.195*	*36.518*	*6*	*5*	*5*	*6.2*	*8.2*	*59.1*	*5.6*	*43.6*	*8.7*	*61.1*	*5.5*	*141.1*	*6.5*	*6.3*	*29.7*			
Yeniköy, Krijgsman et al. (1996)		39.200	36.500	102	88	84	306.2	3.1	26.2	5.1	318.0	3.7	41.5	4.5	22.2	3.4	2.0	5.0			
Inkonak	**Upper Oligocene**	**39.3**	**37.1**	**173**	**98**	**87**					**304.0**	**5.0**	**45.9**	**5.4**	**12.8**	**4.4**	**2.0**	**4.9**	**56.0**	**5.0**	**ccw**
Inkonak		39.315	37.060	173	98	87	314.3	4.2	33.7	6.1	304.0	5.0	45.9	5.4	12.8	4.4	2.0	4.9			
Gemerek	**Miocene**	**39.200**	**36.000**	**99**	**76**	**71**					**310.1**	**3.8**	**36.6**	**5.2**	**23.1**	**3.6**	**2.2**	**5.6**	**49.9**	**3.8**	**ccw**
Gemerek		39.163	36.048	99	76	71	156.4	10.2	66.4	5.0	310.1	3.8	36.6	5.2	23.1	3.6	2.2	5.6			
Bünyan	**Miocene**	**38.1**	**39.9**	**17**	**16**	**16**															
SS24 (recent)		*38.806*	*39.934*	*17*	*16*	*16*	*357.2*	*5.5*	*57.9*	*4.0*	*355.9*	*6.5*	*62.9*	*3.8*	*63.9*	*4.6*	*4.0*	*14.3*			
Sivas	**Miocene**	**39.6**	**37.0**	**102**	**59**	**59**	**13.1**	**4.8**	**57.0**	**3.6**					**25.0**	**3.8**	**2.3**	**6.3**	*16.3*	*4.8*	*cw*
SS12*		39.596	37.036	32	5	5	264.8	10.0	-1.8	20.1	228.5	10.8	-40.6	13.6	60.0	10.0	6.3	29.7			
SS13		39.610	37.027	20	17	17	178.2	4.6	-53.5	3.9	169.5	3.2	-37.5	4.4	139.9	3.0	3.9	13.8			
SS22		39.624	37.018	33	33	33	21.8	5.4	59.1	3.7	10.8	3.4	26.5	5.5	59.7	3.3	3.0	9.1			
SS23		39.603	37.032	17	9	9	199.5	13.9	-52.5	12.2	179.1	11.9	-43.6	13.8	24.1	10.7	5.0	20.5			
Zara	**Miocene**	**39.7**	**37.8**																		
SS35		*39.718*	*37.753*	*11*			*no result*														
SS37		*39.727*	*37.857*	*11*			*no result*														
SS42		*39.700*	*37.752*	*13*			*no result*														
Kemah	**Miocene**	**39.6**	**38.9**	**31**	**14**	**14**	**6.7**	**5.4**	**56.7**	**4.1**					**87.1**	**4.3**	**4.2**	**15.6**	*6.7*	*5.4*	*cw*
SS38		*39.656*	*39.020*	*7*			*no result*														
SS39		39.661	39.020	12	9	9	188.6	8.4	-57.7	6.1	179.1	4.6	-33.3	6.8	137.7	4.4	5.0	20.5			
SS40		*39.612*	*38.829*	*7*			*no result*														
SS41		39.606	38.827	5	5	5	183.5	4.0	-54.9	3.2	136	12.2	-7.55	3.3	190.2	5.6	6.3	29.7			
Kalkar	**Miocene**	**39.2**	**35.9**	**36**	**31**	**27**	**10.1**	**10.3**	**60.0**	**6.8**					**23.4**	**5.5**	**3.1**	**9.6**	*10.1*	*10.3*	*cw*
Kaleköy+Karaözü Langereis et al. (1990)		39.223	35.943	36	31	27	10.1	10.3	60.0	6.8	336.1	5.9	34.3	8.4	23.4	5.5	3.1	9.6			
LITERATURE REVIEW																					
Cappadocia (2,3,10,11)	**Late Miocene-Pliocene**	**38.864**	**33.903**	**80**	**77**						**353.5**	**3.3**	**50.7**	**3.1**	**33.8**	**2.8**	**2.1**	**5.3**	**6.5**	**3.3**	**ccw**
Kırşehir - AAB (9)	**Upper Cretaceous**	**38.910**	**33.810**	**248**	**242**		**331.3**	**2.8**	**49.8**	**2.7**					**14.8**	**2.4**	**1.3**	**2.6**	**28.7**	**2.8**	**ccw**
Kırşehir - KKB (9)	**Upper Cretaceous**	**39.590**	**33.430**	**268**	**266**		**352.8**	**2.6**	**56.3**	**2**					**17.9**	**2.1**	**1.3**	**2.4**	**7.2**	**2.6**	**cw**
Kırşehir - AYB (9)	**Upper Cretaceous**	**39.790**	**34.960**	**66**	**64**		**18.4**	**6**	**54.1**	**5**					**13.8**	**5**	**2.3**	**6**	**18.4**	**6**	**cw**
Kepezdağ (6)	**Miocene (16-14 Ma)**	**38.300**	**37.600**	**10**	**10**						**334.1**	**19.5**	**51**	**18.1**	**9.5**	**16.5**	**4.8**	**19.2**	**25.9**	**19.5**	**ccw**
Yamadağ (6)	**Miocene (18-9 Ma)**	**39.000**	**38.100**	**64**	**61**						**332**	**6.2**	**50.4**	**5.9**	**12.9**	**5.3**	**2.3**	**6.2**	**28**	**6.2**	**ccw**
Eastern Taurides (4,11)	**Middle Eocene**	**38.600**	**36.400**	**80**	**80**						**329.8**	**3.8**	**45.3**	**4.3**	**22.3**	**3.4**	**2.1**	**5.2**	**30.2**	**3.8**	**ccw**
Eastern Taurides Ecemis (11)	**Upper Cretaceous**	**37.400**	**34.900**	**158**	**154**						**318.5**	**3**	**30.4**	**4.7**	**16.1**	**2.9**	**1.6**	**3.4**	**41.5**	**3**	**ccw**
Pontide orocline E limb (5)	**Upper Cretaceous**	**41.300**	**35.400**	**121**	**112**						**32.1**	**4.1**	**40.5**	**5.1**	**13.7**	**3.7**	**1.8**	**4.2**	**32.1**	**4.1**	**cw**
Pontide orocline centre (5)	**Upper Cretaceous**	**41.800**	**33.600**	**77**	**77**						**353.6**	**3.4**	**36.9**	**4.6**	**26.7**	**3.2**	**2.1**	**5.3**	**6.4**	**3.4**	**ccw**
Pontide orocline W limb (5)	**Upper Cretaceous**	**44.400**	**32.100**	**448**	**437**						**334.6**	**1.4**	**44.1**	**1.6**	**28.6**	**1.3**	**1.1**	**1.8**	**25.4**	**1.4**	**ccw**
Eastern Pontides all (4-5, 12-15)	**Upper Cretaceous-Eocene**	**40.600**	**38.400**	**161**	**160**						**359.7**	**2.7**	**42.8**	**3.2**	**22.4**	**2.4**	**1.6**	**3.4**	**0.3**	**2.7**	**ccw**

References:

2: Platzman et al., 1998; 3: Piper et al., 2002; 4: Kissel et al., 2003; 5: Meijers et al., 2010; 6: Gürsoy et al., 2011; 7: Meijers et al., 2011; 8: Lucifora et al., 2012;
9: Lefebvre et al., 2013; 10: Piper et al., 2013; 11: Çinku et al., 2016 12: Baydemir, 1990; 13: Channel et al., 1996; 14: Orbay and Bayburdi, 1979; 15: van der Voo, 1968.

Table 1: Paleomagnetic results presented in this study and localities compiled from literature review.

Lat/Long (°) – latitude/longitude of sites/localities, N_a - number of samples analyzed, N_i - number of samples interpreted, N_{45} number of samples after application of a fixed cut-off (45°), *D* – declination, *I* - inclination; DD_x - declination error, DI_x - inclination error, *K, A95* –

5   Fisher (1953) precision parameter and cone of confidence of 0the mean virtual geomagnetic pole (VGP). $A95_{min}$ and $A95_{max}$ represent the confidence envelope of Deenen et al., (2011). If A95 falls within this envelope the distribution likely represents paleosecular variation. *Rot* = amount of rotation relative to North, *DRot*= uncertainty in amount of rotation; cw = clockwise; ccw = counter-clockwise. Rotations in black (white) are interpreted from a primary (secondary) magnetization. Sites indicated with 'recent' carry a magnetization that has been recently acquired, and are discarded. All site results given in both geographic and tectonic coordinates locality results are given in

10   either geographic or tectonic coordinates depending on our interpretation as explained in the text.

Age (Ma)	n	Latitude	Longitude	A95
10	11	74.5	277.7	8.7
20	15	63.0	290.0	8.6
40	24	65.3	278.4	6.0
50	28	63.3	277.5	5.1
60	9	60.7	276.8	8.2
70	9	64.9	281.5	11.3
80	9	60.8	292.2	9.7
130	4	46.1	289.3	9.0

Table 2: Apparent Polar Wander Path calculated from published and new site averages of SE Anatolia.

Poles integrate site averages from 20 Myr sliding windows, i.e. for the 10 Ma pole, all sites with ages of 0-20 Ma were averaged, etc. n=number of sites. Lat, lon refer to pole latitude and longitude. A95 = cone of confidence around the pole.

Supplementary Information 1: Paleomagnetic data files compatible with Paleomagnetism.org (Koymans et al., 2016) used in this paper. Paleomagnetic demagnetization files are provided in a folder with .dir files, and contain demagnetization diagrams and our interpretations, viewable in the interpretation portal of paleomagnetism.org. The folder with .pmag files contains the statistical parameters of sites and localities discussed in this paper and are provided as separate files for the

10 Ulukışla , Sivas, and Tauride basins. In addition, we provide files with parametrically sampled literature data, compiled from Baydemir, 1990, Channell et al., 1996, Cinku et al., 2016, Gürsoy et al., 2011, Gürsoy et al. 2003, Hisarli et al., 2016, Kissel et al., 2003, Lefebvre et al., 2013, Lucifora, et al., 2012, Meijers et al., 2010 and references therein, Orbay and Bayburdi, 1979, Piper et al., 2002, Piper et al., 2012, Piper et al., 2013, Platzman et al., 1998, Saribudak, 1989, Tatar et al., 2000, Van der Voo, 1968.

Supplementary Information 2: Detailed biostratigraphic constraints obtained from calcareous nannofossils are provided for the Berendi locality in the Central Taurides.